Progress In Electromagnetics Research, PIER 11, 199–253, 1995

A PHYSICAL OPTICS METHOD OF ANALYSIS FOR JUNCTIONS IN DIELECTRIC WAVEGUIDES

S. Safavi-Naeini and Y. L. Chow

1. Introduction

Dielectric waveguide junctions such as steps, abrupt bends, branches, and etc. are building blocks of many optical signal processing devices. In this regard, designing high quality junctions with low transmission and reflection losses, good isolation between branches, and reduced power coupling to unwanted guided modes is an important engineering task in guided wave opto-electronics. Analytical and numerical

techniques for analyzing the behavior of these structures, understanding their deficiencies, and improving their performances are essential for this task.

Junctions and branches in dielectric waveguides have been studied extensively [1–27]. Analytical approximations like those presented in early works [1–3], then in coupled mode theory [6–8], plane wave spectrum (spectral domain) methods [10–13], and in a volume integration technique [14] have been used to treat junction problem. The more rigorous numerical schemes such as "least square boundary residual" method [15–17], integral equation techniques [18,19], Beam Propagation Method (BPM) [20,21], finite and boundary element method [22], iterative procedure [23], and Finite Difference Time Domain (FD/TD) [24] have also been applied to this problem.

The approximate analytical methods mentioned above usually have a fairly limited scope of application. For example, it is difficult to analyze wide angle Y-branches or large step junctions with non-negligible reflection by coupled mode theory or by simple mode matching formulas [1–3]. On the other hand, numerical techniques, although accurate and more general, require a considerable amount of computer resources (CPU time and memory) and often do not provide the user with sufficient insight in the problem. Therefore they are not appropriate for design and optimization purposes.

The new physical optics (P.O.) method of this chapter, developed recently in [25–27] is a simple analytic approximate technique. It is based on the waveguide modal excitation from the junction interface P.O. fields.

The physical optics method often leads to closed form expressions for transmission and reflection coefficients. As a result the present P.O. method is simpler and more efficient than other numerical schemes and approximate methods, e.g., volume current integration [14] and plane wave spectrum approaches [10–13].

Like the purely geometrical ray theory [28] this method gives much physical insight and is very versatile for arbitrary structures. However, the method does not suffer from the deficiencies (e.g., sharp shadows) of pure ray theory.

Modal wave propagation in a *uniform* section of a waveguide can be represented by a sum of plane wave (modal) rays exactly. However, the transmission of lightwaves through arbitrary waveguide junctions containing *finite* dielectric interfaces cannot accurately be modeled by

simple plane wave ray reflection and refraction from an *infinite planar* interface.

In the present method, the above modal rays are employed only to estimate the fields at the interface by P.O. approximation. The latter are then used in a *rigorously* derived field integral for the junction transmission. The method, therefore, does take the finiteness of dielectric interfaces into account and is less susceptible to localized irregularities of the interface field. In this respect, it combines the simplicity and intuition provided by the ray concept, with the mathematical rigor of electromagnetic wave theory. In the future, one can still improve the accuracy systematically by including the known behavior of the field over the critical parts such as corners of the interface in the P.O. estimates.

To describe the method, in section 2 and 3 we concentrate on the configuration shown in Fig. 1. Then applications to more general 2-D structures (step, bend, and Y-junction) are described in Sections 4, 5, and 6. A new low loss abrupt bend configuration and its design criteria are discussed in Section 6. The P.O. analysis of (3-D) structures is finally discussed in Section 8.

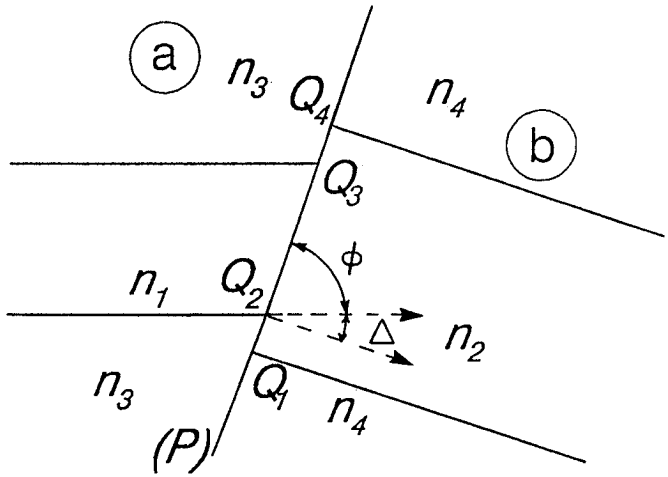

Figure 1. A general junction between two dielectric waveguides.

2. Physical Optics Estimation of the fields over a Dielectric Interface

In this section after a brief review of the physical optics, its application to dielectric interfaces contained in the junction shown in Fig. 1 is detailed.

2.1 Basic Concepts of Physical Optics

Physical optics is an approximate method for finding the field scattered by an object from the knowledge of the field on its surface. In its application to conducting (impenetrable) bodies the surface field at each point on the *geometrically illuminated side* is taken to be that due to the incident wave scattered by an infinite plane tangent to the surface at that point [29]. On the *geometrical shadow side* the surface field is assumed to be zero. Physical optics field is therefore expressed by a radiation type integral over the illuminated part of the surface. Extensions to bodies with impedance surface and dielectric bodies have also been reported [30,31].

For large (in terms of wavelength) smooth convex bodies, the above physical optics integral can be asymptotically expanded via steepest descent method. The first term is the geometrical optics field which is also equal to the leading term of the asymptotic expansion of the exact solution (Luneburg-Kline expansion [32]). In this sense physical optics may be viewed as a generalization of the geometrical optics and as such should provide us with more accurate estimates of fields.

In this section, we apply physical optics to determine the fields scattered by and transmitted through the interface plane (P) in the region (b) of Fig. 1 due to the incident field coming from the region (a). According to the equivalence principle, the fields in the region (b) may be viewed as being generated by the equivalent magnetic and electric currents $(\vec{J}_P^{eq}, \vec{M}_P^{eq})$ placed on (P). Estimates of these currents are obtained through a simple extension of the conventional physical optics (P.O.) to dielectric bodies. These estimates (physical optics sources) are denoted by $\vec{J}^{PO}$ and $\vec{M}^{PO}$. Currently the physical optics (P.O.) method is widely used to calculate the *far* scattered or radiated fields in open space. In the present application, however, we employ physical optics estimates for the surface fields to determine the amplitudes of the

transmitted and reflected *guided (bound) modes* via an inner product integration (9 and 10) over the junction interface.

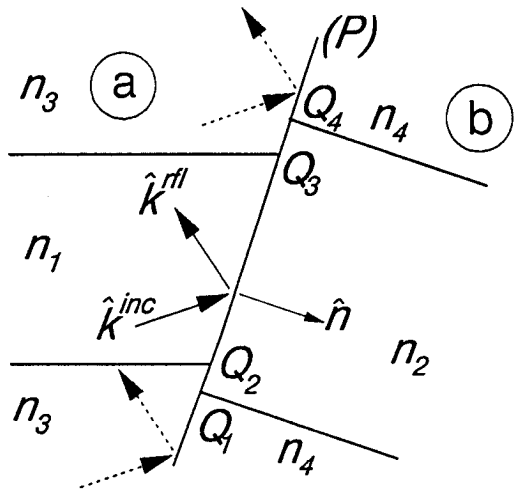

Figure 2. Incident and reflected (plane wave) rays at the junction interface (P).

2.2 Physical Optics Approximation for the Fields on a Dielectric Waveguide Junction Interface

We apply the above principles to the specific junction of Fig. 1. The neighborhood of the interface plane (P) is illustrated in Fig. 2.

According to the basic postulate of physical optics [29], the fields at each point of P are approximately those due to incident wave reflected and refracted by an infinite dielectric planar interface tangent to the surface P at that point.

In contrast to its application to conducting objects, for dielectric interfaces, physical optics sources are of both electric and magnetic types. If the incident and reflected fields in region a are denoted by $(\vec{E}^{inc}, \vec{H}^{inc})$ and $(\vec{E}^{rfl}, \vec{H}^{rfl})$ respectively, these sources are currents given by:

$$\vec{J}^{PO} = \hat{n} \times (\vec{H}^{inc} + \vec{H}^{rfl}), \vec{M}^{PO} = -\hat{n} \times (\vec{E}^{inc} + \vec{E}^{rfl}) \qquad (1)$$

where $\hat{n}$ is the unit vector normal to the interface plane P.

In Figure 2 one may notice that dielectric waveguides join along a planar surface (interface) P and the incident wave can be represented by a finite sum of plane waves in each homogeneous region. In this case the determination of the above physical optics sources is particularly simple. The incident fields ($\vec{E}^{inc}, \vec{H}^{inc}$) may now represent any plane wave ray constituent of the incident modal wave(s) coming along the waveguide a which give rise to reflected plane wave ($\vec{E}^{rfl}, \vec{H}^{rfl}$) upon reflection at the dielectric interface.

At a point $\vec{r}_P$ on the interface (P) each plane wave ray constituent of the incident field, polarized along $\hat{u}$ with the wave vector $\vec{k}_a^{inc}$ is:

$$\vec{E}^{inc} = \vec{E}_0^{inc} exp(-j\vec{k}_a^{inc} \cdot \vec{r}_P), \vec{H}^{inc} = \hat{k}_a^{inc} \times \frac{\vec{E}^{inc}}{\eta_a} \tag{2}$$

the corresponding reflected wave is:

$$\vec{E}^{rfl} = \vec{E}_0^{rfl} exp(-j\vec{k}_a^{rfl} \cdot \vec{r}_P), \vec{H}^{rfl} = \hat{k}_a^{rfl} \times \frac{\vec{E}^{rfl}}{\eta_a} \tag{3}$$

where,

$$\vec{k}_a^{rfl} = \vec{k}_a^{inc} - 2(\vec{k}_a^{inc} \cdot \hat{n})\hat{n} \tag{4}$$

and $\hat{n}$ is the unit normal of the interface into the region a, and the reflected field vector, $\vec{E}_0^{rfl}$, is related to the incident field $\vec{E}_0^{inc}$ components through a reflection coefficient given in the Appendix. Detail uses of the reflection coefficients are demonstrated in the examples of the following section.

The unit vectors $\hat{k}_a^{inc,rfl}$ are defined along the wave vectors $\vec{k}_a^{inc,rfl}$ in the region a and $\eta_a = \sqrt{(\mu_a/\epsilon_a)}$ is the wave characteristic impedance. It is reemphasized that as one moves along the interface, the reflection coefficients giving $\vec{E}_0^{rfl}, \vec{k}_a^{inc,rfl}$, and η_a , in general, are not constant and should be defined locally.

The incident and reflected *plane wave ray* fields of (2), (3) (with the parameters defined in the Appendix), substituted back in (1), provide us with the physical optics sources generated by *one* plane wave constituent of the incident modal field. To determine the total P.O. sources, the contributions of all constituents should be summed up.

It is obvious from the expressions (1,2,3) that physical optics sources have "non-physical" discontinuities at the junction points Q_1, Q_2, Q_3, and Q_4. In addition, possible physical singularities of the normal (to the wedge axis) components of the fields [33,34] have not been

taken into account in the above estimates. Nevertheless, in optical waveguide structures the relative index change across the interfaces are usually small and so are these deviations of P.O. fields from the true behavior of the fields. It is also to be pointed out that such non-physical behaviors or singularities are weak and *localized* in nature. Therefore the resulted errors in the final results remain insignificant.

It is to be mentioned that the *plane wave ray* model employed throughout this chapter is a an approximate but accurate mean to estimate the interface fields. These are then used in the field integral expressions for the amplitudes of the excited propagating modes in various regions.

To represent *wave packet* processes and flow of energy in dielectric waveguides, ray should be defined in a more precise manner. In such cases, the ray *does not* coincide with the propagation vectors of the modal plane waves given in (2) and (3). This difference in directions causes the *lateral shift* (Goos-Hanchen shift) [38] of the reflected ray relative to the incident ray. Nevertheless, as will be shown in later Sections, for monochromatic field (especially the phase) estimations required in this chapter, the simple *plane wave* ray model of this section, provides us with an adequate field representation with a great practical appeal.

In the later Sections the physical optics estimates for the interface fields will be derived for specific structures of practical interest such as steps, abrupt bends, and Y-junctions.

3. Formulation of Dielectric Waveguide Junction Problem in terms of the Junction Interface Fields

In this Section we formulate the power transmission analysis of a general dielectric waveguide junction shown in Fig. 1 in terms of the tangential fields over the junction interface plane. The method, however, can be applied to more general type of discontinuities in guiding structures, as shown in the later sections.

The abrupt junction in Fig. 1 is formed by two different dielectric waveguide meeting along the planar interface (P). The core (guiding region) refractive indices are n_1 and n_2 and those of the claddings are n_3 and n_4 for the waveguides a and the waveguide b respectively. The interface plane (P) has the angle ϕ with the axis z of the waveguide

a. The bending angle between the two waveguides is denoted by Δ. Various types of abrupt bends and steps explained in the Sections 4 and 5 are special cases of this general structure.

The specific problem addressed in this section is:*the determination of the power coupled to various modes in the waveguide b, power reflected by guided modes in waveguide a, and the radiation loss, when a guided mode of unit power in the waveguide a is propagating towards the junction.*

The approach is based upon i) using the tangential interface (P) fields as the equivalent sources for the transmitted and reflected fields in the waveguides *b* and *a* respectively and ii) invoking *electromagnetic reciprocity* to find the amplitudes of the guided modes there.

3.1 Equivalence Theorem

According to electromagnetic equivalence principle (i.e., a theorem) [35], the fields outside some closed surface can be determined uniquely from the knowledge of the tangential electric and magnetic fields on that surface.

To apply this theorem to the specific geometry of Fig. 1 (*original* problem), the interface (P) may be considered to be a portion of a very large surface enclosing the waveguide medium *a*. The fields in the medium *b* of the original problem (Figure 1) can be proven [35] to be the same as those generated by the *equivalent* electric ($\vec{J}_P^{eq}$) and magnetic ($\vec{M}_P^{eq}$) sources located on (P) in the *equivalent* problem illustrated in Fig. 3. According to equivalence theorem these sources are given as:

$$\begin{aligned} \vec{J}_P^{eq} &= \hat{n} \times \vec{H}_P \\ \vec{M}_P^{eq} &= -\hat{n} \times \vec{E}_P \end{aligned} \tag{5}$$

where $\vec{E}_P$ and $\vec{H}_P$ are the total (incident plus scattered) fields on the interface plane (P) and $\hat{n}$ is the unit normal to this plane pointing towards the medium *b*. After the application of (5) the region on the left of the plane P in the equivalent problem (Figure 3) may now be filled with any medium. A simple choice made in Fig. 3 is to replace the waveguide medium *a* by a continuation of the waveguide *b* to the left. The resulted configuration for the equivalent problem in Fig. 3 is much simpler than the original structure (Figure 1). The original

problem (Figure 1) has thus been converted to one of dielectric waveguide excitation by a planar source distribution (Figure 3).

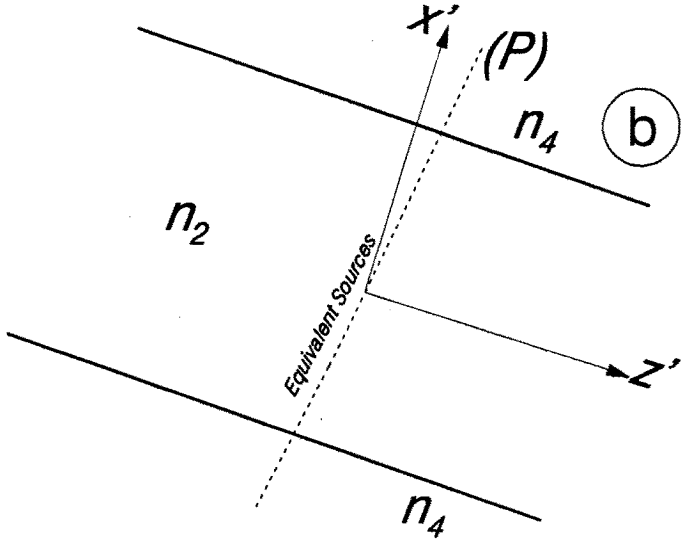

Figure 3. Equivalent problem for the transmitted waves to the waveguide b.

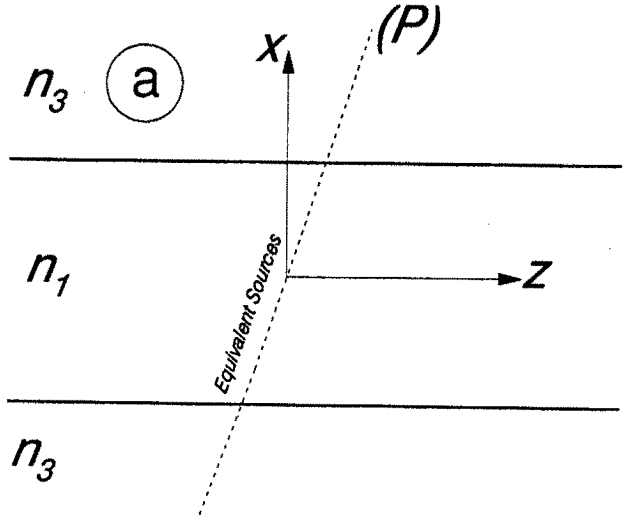

Figure 4. Equivalent problem for the reflected (modal) waves in the waveguide a.

The same procedure can be used for the determination of the power reflected by the guided mode(s) in waveguide a (Figure 4). In this case, according to equivalence theorem, the reflected modal waves in waveguide a of the original structure are the same as those generated by the sources $(-\vec{J}_P^{eq}, -\vec{M}_P^{eq})$ and propagating to the left of the source plane P.

With the above equivalent sources we shall use the following electromagnetic reciprocity to find the modal amplitudes of the fields.

3.2 Reciprocity Expressions For the Power Transmission and Reflection Coefficients

The electric field $\vec{E}_b$ and magnetic field $\vec{H}_b$ in the dielectric waveguide b generated by the equivalent sources on the *right* of (P) in Fig. 3, can be represented in terms of a finite number of *guided (bound)* modes $\{\vec{E}_{bp}^{\pm}, \vec{H}_{bp}^{\pm}\}$ and an infinite number of *radiation (unbound)* modes $\{\vec{E}_{b\nu}, \vec{H}_{b\nu}\}$ as below [36]:

$$\begin{aligned}\vec{E}_b &= \sum_{p\in M_b} B_p^{\pm}\vec{E}_{bp}^{\pm} + \int_{RadiationSpectrum} B(\nu)\vec{E}_{b\nu}d\nu \\ \vec{H}_b &= \sum_{p\in M_b} B_p^{\pm}\vec{H}_{bp}^{\pm} + \int_{RadiationSpectrum} B(\nu)\vec{H}_{b\nu}d\nu\end{aligned} \tag{6}$$

where $(+)$ and $(-)$ signs denote respectively propagation to the *right* and *left* of the plane P. For 3-D guides (channel, ribs, etc.), the modal index p is an ordered pair of integers, M_b is a finite set of the guided mode indices, and the radiation part is a 2-D integral over a 2-D continuous spectrum of ν. In the case of slab waveguides (2-D structure), the above expansion involves only 1-D summations and integrals of ν.

The propagation in waveguide b is taken to be along its axis z'. The translational invariance along the same direction allows us to express propagating modes as:

$$\begin{aligned}\vec{E}_{bp}^{\pm} &= [\vec{e}_{bp}(\vec{\rho}) \pm e_{bpz}(\vec{\rho})\hat{z}']exp(\mp j\beta_{bp}z') \\ \vec{H}_{bp}^{\pm} &= [\pm\vec{h}_{bp}(\vec{\rho}) + h_{bpz}(\vec{\rho})\hat{z}']exp(\mp j\beta_{bp}z')\end{aligned} \tag{7}$$

where $\vec{\rho}$ is a position vector in the transverse (perpendicular to $\hat{z}'$) plane, β_{bp} is the propagation constant of the mode p, and $\{\vec{e}_{bp}, \vec{h}_{bp}\}$

are transverse field vectors of the waveguide b. The temporal variation of the fields is $\exp(-j\omega t)$.

Determination of modal expansion coefficients $B_p^{\pm}, B(\nu)$ requires *orthogonality relation* between modes. A general form of this relation is given below [37]:

$$\int_{S_b} \vec{e}_{bp} \times \vec{h}_{bq} \cdot \hat{z}' d_2\vec{\rho} = \int_{S_b} \vec{e}_{bq} \times \vec{h}_{bp} \cdot \hat{z}' d_2\vec{\rho} = 0; \quad p \neq q \tag{8}$$

where S_b is the transverse cross section plane of the waveguide b. The relation holds between any two forward propagating $(+)$ modes, any two backward propagating $(-)$ modes, and between one guided and one radiation mode. In the latter case, one of the modal transverse vectors in (8) can be replaced by one radiation mode. Two radiation modes with different propagation constants are also orthogonal.

The unknown amplitudes $\{B_p^+\}$ and the continuous spectrum $B(\nu)$ can be found in terms of the equivalent sources given in (1) through *electromagnetic reciprocity.*

Following [37], we use the reciprocity relation between the field generated by the above sources and the source-free modal fields of the waveguide b combined with the orthogonality relation (8), to derive the amplitudes of the guided modes in the waveguide b:

$$\begin{aligned} B_p^+ &= -\frac{1}{2N_{bp}} \int_{(P)} (\vec{E}_{bp}^- \cdot \vec{J}_P^{eq} - \vec{H}_{bp}^- \cdot \vec{M}_P^{eq}) d_2\vec{r}_P \\ N_{bp} &= \int_{S_b} (\vec{e}_{bp} \times \vec{h}_{bp}) \cdot \hat{z}' d_2\vec{\rho} \end{aligned} \tag{9}$$

where $\vec{r}_P$ is a position vector on the interface plane (P).

If the modes of waveguide $b\{\vec{e}_{bp}, \vec{h}_{bp}\}$ are normalized to *unit* power, then the $B_p^{+'}s (p \in M_b)$ give the *coupling coefficients* between the input *unit* power mode coming along the waveguide a and the p-th excited guided mode in waveguide b. In this case the power transmission ratios are $|B_p^+|^2$.

A similar procedure can be followed for determining the amplitude of the reflected guided modes in the waveguide a. The equivalent problem illustrated in Figure 4 should be employed this time. The equivalent sources are now radiating in waveguide a environment to the left of the plane (P). The amplitude A_p^- of the reflected mode

$\{\vec{E}_{ap}^{-}, \vec{H}_{ap}^{-}\}(p \in M_a; M_a$ is the finite set of the guided mode indices) in waveguide a may now be written as:

$$A_p^- = -\frac{1}{2N_{ap}} \int_{(P)} (\vec{E}_{ap}^{+} \cdot \vec{J}_P^{eq} - \vec{H}_{ap}^{+} \cdot \vec{M}_P^{eq}) d_2\vec{r}_P \tag{10}$$

where N_{ap} is similar to N_{bp} in (9). Here again if the reflected modes are normalized to unit power, the power reflection ratios are given by $|A_p^-|^2$.

Having determined the powers transmitted and reflected by guided modes, the power lost in radiation (radiation loss) L_{rad} can be found as:

$$L_{rad} = 1 - \sum_{p \in M_b} |B_b^+|^2 - \sum_{q \in M_a} |A_q^-|^2 \tag{11}$$

To determine various coupling coefficients and power ratios by (10) and (9) the fields on the interface surface P, due to the incident guided mode in the waveguide a need to be known. The exact knowledge of these fields requires *rigorous* solution of the wave equation which can be complicated. An accurate estimate of the interface fields (equivalent sources), however, can be obtained by the physical optics procedure explained in the previous Section.

The physical optics approximation proposed in this work essentially consists of estimating the $\{\vec{J}_P^{eq}, \vec{M}_P^{eq}\}$ in rigorous expressions (10) and (9) by the physical optics sources:

$$\begin{aligned} \vec{J}_P^{eq} &\approx \vec{J}^{PO} \\ \vec{M}_P^{eq} &\approx \vec{M}^{PO} \end{aligned} \tag{12}$$

The application of the method to specific guiding structures is detailed in the next few Sections.

4. Step Junction of Dielectric Waveguides (2-D)

As the first example we study the power reflection and transmission ratios of the step junction between two *symmetric* dielectric slab waveguides shown in Fig. 5. This is a special 2-D version of the configuration shown in Fig. 1
where $\Delta = 0°, \phi = 90°$. There is no variation along the y-axis which is taken to be perpendicular to the plane of Fig. 5.

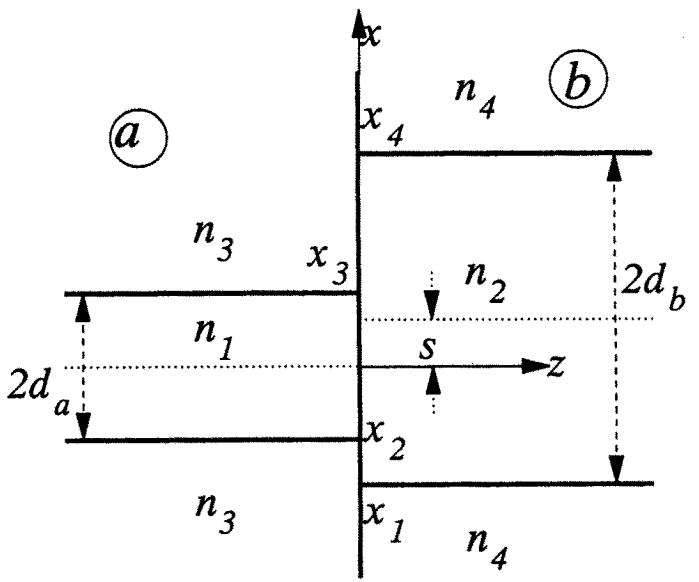

Figure 5. A step junction between two parallel (2-D) slab waveguides.

The incident field and its (plane wave) ray representation are discussed first. These rays are then used to find physical optics sources and thereby determine the amplitudes of the transmitted and reflected modes.

4.1 Incident Field

The incident field is a modal wave (fundamental mode in this example) in the waveguide a propagating towards the junction at z = 0. The coordinate z is defined along the axis of the waveguide a. The latter has a parallel displacement of s with respect to the axis of the waveguide b. The coordinate x is along the interface plane (P). With these defined, the main components of the TE and TM fields are given below.

The components of a unit power TE wave (fundamental mode) $(\vec{E}^+_{a1}, \vec{H}^+_{a1})$ are:

$$E^+_{a1y} = e_{a1y}e^{-j\beta_a z}$$

$$= \begin{cases} C_1 \cos(\tau_a x)\exp(-j\beta_a z) & |x| < d_a \\ C_1 \cos(\tau_a d_a)\exp[-\alpha_a(|x| - d_a) - j\beta_a z] & |x| > d_a \end{cases} \tag{13}$$

$$H^+_{a1x} = h_{a1x}e^{-j\beta_a z} = -\frac{\beta_a}{\omega\mu}E^+_{a1y}$$

$$H^+_{a1z} = h_{a1z}e^{-j\beta_a z} = -\frac{j}{\omega\mu}\frac{\partial E^+_{a1y}}{\partial x}$$

where C_1 is the (unit power) normalization constant for the fundamental mode. The modal propagation constant along $\hat{z}$ has been denoted by β_a and the other parameters are shown in Fig. 5. The wave parameters $(\tau_a, \beta_a, \alpha_a)$ are found from the TE modal dispersion relations [38, 39]:

$$\begin{aligned} \beta_a^2 &= n_1^2 k_0^2 - \tau_a^2 = n_3^2 k_0^2 + \alpha_a^2 \\ \alpha_a &= \tau_a \tan(\tau_a d_a) \end{aligned} \tag{14}$$

Similar expressions exist for a unit power TM incident wave after substitutions of $\{E^+_{a1y} \to H^+_{a1y}, H^+_{a1z} \to -E^+_{a1z}, H^+_{a1x} \to -E^+_{a1x}, \mu \to \epsilon\}$ and using the TM dispersion relations:

$$\begin{aligned} \beta_a^2 &= n_1^2 k_0^2 - R_a^2 = n_3^2 k_0^2 - r_a^2 = n_3^2 k_0^2 + \alpha_a^2, \\ n_1^2 \alpha_a &= n_3^2 \tau_a \tan(\tau_a d_a) \end{aligned} \tag{15}$$

4.2 P.O. Estimates of the Tangential Fields over the Junction Interface

The following gives the P.O. fields over the junction interface for TE polarization. The corresponding fields for TM waves are similar. Determination of physical optics sources requires the representation of guided modes in terms of a number of homogeneous or inhomogeneous plane wave rays. For the 2-D dielectric slab waveguides below, this representation is exact.

The Core region

Inside the core region ($|x| < d_a$) the incident field (Eq. 13) can be written as the sum of two *homogeneous* plane waves propagating along directions which make angles $\pm\delta_a = \pm\tan^{-1}(\tau_a/\beta_a)$ with the z-axis. The incident and reflected (from the junction interface) plane wave rays are:

$$\vec{E}^{inc}_{\pm\delta_a} = \hat{y}\frac{C_1}{2}e^{\mp j\tau_a x - j\beta_a z} \tag{16}$$

These rays after reflecting back from the junction interface (P) at x give rise to reflected plane wave rays:

$$\vec{E}^{rfl}_{\pm\delta_a} = \hat{y}R^{TE}(x,\pm\delta_a)\frac{C_1}{2}e^{\mp j\tau_a x + j\beta_a z} \tag{17}$$

where $R^{TE}(x,\pm\delta_a)$ is the *local* TE plane wave reflection coefficient at x on the interface when the incidence direction makes angle $\pm\delta_a$ with the z-axis. The general expression (55) for R^{TE} given in the Appendix can be rewritten as a function of x as below:

$$R^{TE}(x,\pm\delta_a) = \frac{n_a(x)\cos(\pm\delta_a) - [n_b(x)^2 - n_a(x)^2\sin^2(\pm\delta_a)]^{\frac{1}{2}}}{n_a(x)\cos(\pm\delta_a) + [n_b(x)^2 - n_a(x)^2\sin^2(\pm\delta_a)]^{\frac{1}{2}}} \tag{18}$$

The above expression is the reflection coefficient at the planar interface between two semi-infinite media of refractive indices $n_a(x)$ and $n_b(x)$ illuminated from the $n_a(x)$ side. Depending upon x, n_a and n_b may assume values (n_1, n_3) and (n_2, n_4) respectively. For the example shown in Fig. 5, when $x_2 < x < x_3, n_a(x) = n_1$ and $n_b(x) = n_2$. It is noted that for step junction, since $\phi = 90°$, $R^{TE}(x,\delta_a) = R^{TE}(x,-\delta_a)$.

To find the P.O. estimate of the total field $\vec{E}^{PO}_P(x)$ at a typical point x on the interface surface P, following the procedure of the Section 2.2, the reflected waves at x are added to the incident plane waves:

$$\begin{aligned}\vec{E}^{PO}_P(x) =& \vec{E}^{inc}_{+\delta_a} + \vec{E}^{inc}_{-\delta_a} + \vec{E}^{rfl}_{+\delta_a} + \vec{E}^{rfl}_{-\delta_a}\\ =& \hat{y}\frac{C_1}{2}\left\{\left[1 + R^{TE}(x,\delta_a)\right]e^{-j\tau_a x}\right.\\ &\left. + \left[1 + R^{TE}(x,-\delta_a)\right]e^{j\tau_a x}\right\}\end{aligned} \tag{19}$$

Having found the incident and reflected electric fields, the magnetic field counterparts are obtained from (2) and (3). The P.O. estimate for

the total x-component (tangential) magnetic field at the point x on the interface, $H_{Px}^{PO}(x)$, inside the core $(x_2 < x < x_3)$ is:

$$\begin{aligned} H_{Px}^{PO}(x) =& \hat{x} \cdot (\vec{H}_{+\delta_a}^{inc} + \vec{H}_{-\delta_a}^{inc} + \vec{H}_{+\delta_a}^{rfl} + \vec{H}_{-\delta_a}^{rfl}) \\ =& \beta_a \frac{\lambda}{240\pi^2} \frac{C_1}{2} \left\{ \left[1 - R^{TE}(x, \delta_a)\right] e^{-j\tau_a x} \right. \\ & \left. + \left[1 - R^{TE}(x, -\delta_a)\right] e^{j\tau_a x} \right\} \end{aligned} \tag{20}$$

The cladding region

In the cladding $(|x| > d_a)$ the interface field at each point is again found by summing up the incident and reflected fields as detailed before. The only difference is that in this case the fields are inhomogeneous plane waves defined as:

$$\vec{E}_{\pm\gamma_a}^{inc} = \hat{y} C_1 \cos(\tau_a d_a) e^{\alpha_a d_a} e^{\mp\alpha_a x - j\beta_a z} \tag{21}$$

$$\vec{E}_{\pm\gamma_a}^{rfl} = \hat{y} R^{TE}(x, \pm\gamma_a) C_1 \cos(\tau_a d_a) e^{\alpha_a d_a} e^{\mp\alpha_a x - j\beta_a z} \tag{22}$$

where $\gamma_a = -\sin^{-1}[j\alpha_a/(n_3 k_0)]$ is the *complex* incident angle (with respect to z-axis) of the *inhomogeneous* plane waves in the cladding. The signs (+)and (-) refer to the regions $x > d_a$ and $x < -d_a$ respectively. In fact, the fields in the cladding may be viewed as plane wave rays with complex phases. These can be derived from general plane wave expressions (2) and (3) using properly defined *complex* wave vectors:

$$\begin{aligned} \vec{k}_{\pm\gamma_a}^{inc} &= \mp j\alpha_a \hat{x} + \beta_a \hat{z} \\ \vec{k}_{\pm\gamma_a}^{rfl} &= \mp j\alpha_a \hat{x} + \beta_a \hat{z} \end{aligned} \tag{23}$$

for the incident rays having complex angles $\pm\gamma_a$ relative to $\hat{z}$ in the cladding cover $(x > d_a)$ and cladding substrate $(x < -d_a)$ regions respectively and their corresponding reflected waves. Unlike the guiding region $(|x| < d_a)$ where we had *two* modal rays, in each cladding region (cover or substrate) there is only one inhomogeneous plane wave ray for each mode.

It is noted that calculation of $R^{TE}(x, \pm\gamma_a)$ in (21) and (22) by the expression (18) requires the "analytical continuation" of this expression

for complex values of δ_a. The proper branch of R^{TE} should be chosen using the knowledge of the physically correct behavior of the fields far from the junction. It can easily be shown that with this proper analytical continuation, the expression in (18) is identical to the general formula (51) given in the Appendix. It is also to be mentioned that unlike the core region, here, n_b varies with x. For the geometry shown in Fig. 5, we have:

$$n_a(x) = n_3 \tag{24}$$

$$n_b(x) = \begin{cases} n_4, & x > x_4 \\ n_2, & d_a = x_3 < x < x_4, x_1 < x < x_2 = -d_a \\ n_4, & x < x_1 \end{cases} \tag{25}$$

From (21) and (22), we can write the physical optics estimates for the tangential fields $(E_{Py}^{PO}, H_{Px}^{PO})$ on the interface (P) in the cover $(+)$ and substrate $(-)$ regions as:

$$\begin{aligned} E_{Py}^{PO\pm} &= C_1 \cos(\tau_a d_a)[1 + R^T(x, \pm\gamma_a)]e^{\alpha_a(d_a \mp x)} \\ H_{Px}^{PO\pm} &= -\beta_a \frac{\lambda}{240\pi^2} C_1 \cos(\tau_a d_a)[1 - R^T(x, \pm\gamma_a)]e^{\alpha_a(d_a \mp x)} \end{aligned} \tag{26}$$

4.3 Transmission and Reflection Coefficients in terms of the Tangential Fields

The amplitudes of the normalized (unit power) TE guided modes B_m^{e+} (waveguide b) and the reflected (fundamental) mode A_1^{e-} (waveguide a) derived from (10) and (9) and physical optics sources (1) obtained from (19),(20), and (26) are given below:

$$\begin{aligned} B_m^{e+} &= \frac{(\beta_a + \beta_b)\lambda_0}{480\pi^2 N_{bm}} \int_{-\infty}^{\infty} [1 - R^{TE}(x, \Omega)\Gamma^e] e_{a1y}(x) e_{bmy}(x) dx \\ A_1^{e-} &= \frac{\beta_a \lambda_0}{240\pi^2 N_{a1}} \int_{-\infty}^{\infty} R^{TE}(x, \Omega)[e_{a1y}(x)]^2 dx \\ \Gamma^e &= \frac{\beta_a - \beta_b}{\beta_a + \beta_b} \end{aligned} \tag{27}$$

where $\{e_{amy}\}$ and $\{e_{bmy}\}$ are transverse modal distributions for the electric fields in the waveguides a and b respectively (see Eq. 7). The superscript e denotes the TE polarization and the normalization constants (N_{bm}, N_{a1}) are defined in connection with (9) and (10). The incident angle Ω is defined as:

$$\Omega = \begin{cases} \delta_a, & x_2 < x < x_3 \\ \gamma_a, & x < x_2, x > x_3 \end{cases} \tag{28}$$

The corresponding coupling (B_m^{h+}) and the reflection (A_1^{h-}) coefficients for the TM polarization are derived in a similar manner. The results are:

$$\begin{aligned} B_m^{h+} &= -\frac{30\lambda_0}{N_{bm}} \int_{-\infty}^{\infty} \left(\frac{\beta_a}{n_a^2(x)} + \frac{\beta_b}{n_b^2(x)} \right) \\ &\quad \cdot [1 - R^{TM}(x,\Omega)\Gamma^h(x)] h_{a1y}(x) h_{bmy}(x) dx \\ A_1^{h-} &= -\frac{60\lambda_0\beta_a\lambda_0}{N_{a1}} \int_{-\infty}^{\infty} \frac{R^{TM}(x,\Omega)}{n_a^2(x)} [h_{a1y}(x)]^2 dx \\ \Gamma^h &= \frac{\beta_a/n_a^2(x) - \beta_b/n_b^2(x)}{\beta_a/n_a^2(x) + \beta_b/n_b^2(x)} \end{aligned} \tag{29}$$

where h_{a1y} and h_{bmy} are the magnetic fields of the fundamental TM mode in the waveguide a and the m-th mode in waveguide b respectively. In analogy with $R^{TE}(x,\Omega)$ for TE case discussed above, the local reflection coefficient $R^{TM}(x,\Omega)$ is given here for TM polarization:

$$R^{TM}(x,\Omega) = \frac{\cos(\Omega)/n_a(x) - [1 - n_a(x)^2 \sin^2(\Omega)/n_b^2]^{\frac{1}{2}}/n_b(x)}{\cos(\Omega)/n_a(x) + [1 - n_a(x)^2 \sin^2(\Omega)/n_b^2]^{\frac{1}{2}}/n_b(x)} \tag{30}$$

where the incident angle Ω with respect to the normal to the interface plane P is defined in (28) and, as it has been discussed earlier in connection with relation (27), may take real or complex values. The expression (30) is derived from (51,55) in the Appendix.

It is worth mentioning that the integrals in (27) and (29) can be calculated analytically with closed form results [40]. This indicates very high computational efficiency of the method.

4.4 Sample Applications and Comparison with other Methods

In Figures 6 to 9, transmission and reflection coefficients as predicted by (27) and (29), are compared with those obtained by other methods for some typical step junctions in dielectric slab waveguides.

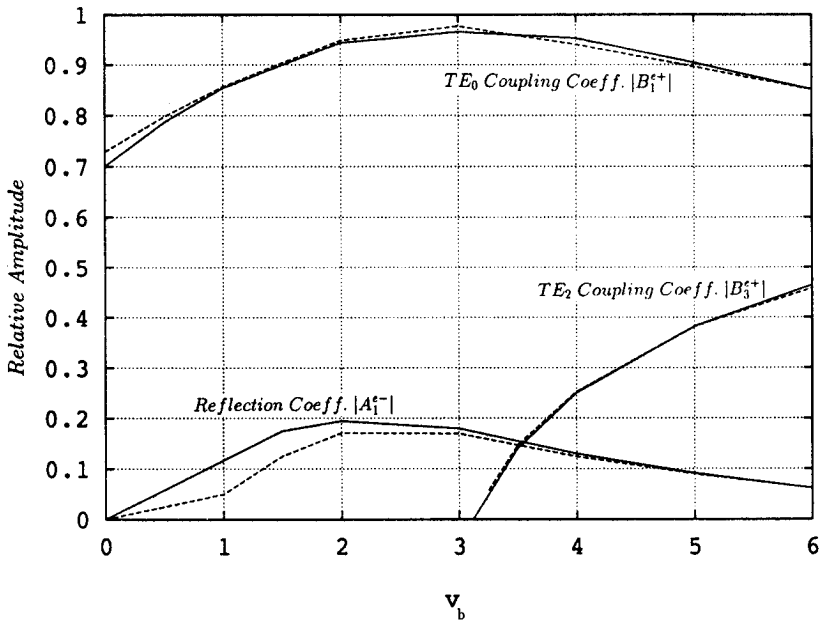

Figure 6. The fundamental mode reflection coefficient ($|A_1^{e-}|$) of the waveguide a and the transmission coefficients ($|B_1^{e+}|$,($|B_2^{e+}|$)) for the first two modes of the waveguide b for the junction of Figure 5 when: $d_a/d_b = 0.2$, $n_1 = n_2$, $n_3 = n_4 = 1$, $s = 0$, and $n_2 k_0 d_b = 1$, obtained by the P.O. method (dotted line) and the integral equation approach (solid line). The normalized frequency of waveguide b, $V_b = k_0 d_b (n_2^2 - n_4^2)^{-1/2}$.

A *symmetrical* step between two dielectric slabs with largely different widths are studied in Figs. 6 and 7. The fundamental TE mode is coming along the waveguide a. The reflection coefficient A_1^{e-} (plot "TE_1^a") of the waveguide a and the transmission coefficients B_1^{e+} (plot "TE_1^b") and B_1^{e+} (plot "TE_2^b") for the first and second modes in the waveguide b as a function of normalized frequency are shown in Fig. 6. The Figure 7 illustrates variation with d_a of the reflection coefficient, transmission coefficient (fundamental mode), and the radiation

loss given in (11) for the same junction when $n_2 k_0 d_b = 1$ and $V_b = 2$. As it is obvious from the Figs. 6 and 7, the numerical results of the present (physical optics) method agrees very well with those generated by a more rigorous integral equation approach [18]. Although the physical optics estimate for the interface field (see Section 2) is essentially a short wavelength approximation, they have produced accurate results even when the wavelength is considerably larger than the slab width in Figure 7 ($n_1 k_0 d_1 < 0.2$).

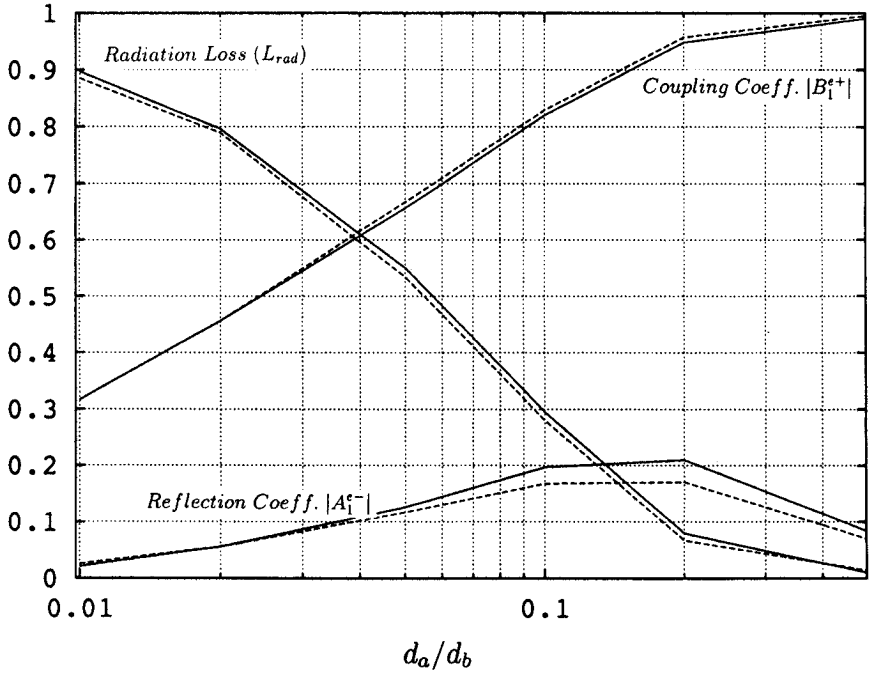

Figure 7. The fundamental mode reflection coefficient ($|A_1^{e-}|$) of the waveguide a, the transmission coefficient ($|B_1^{e+}|$) of the waveguide b, and the radiation loss (Eq. 11) for the junction of Figure 6 when $V_b d_b = 2$. obtained by two methods: P.O. (dotted line) and the integral equation approach (solid line).

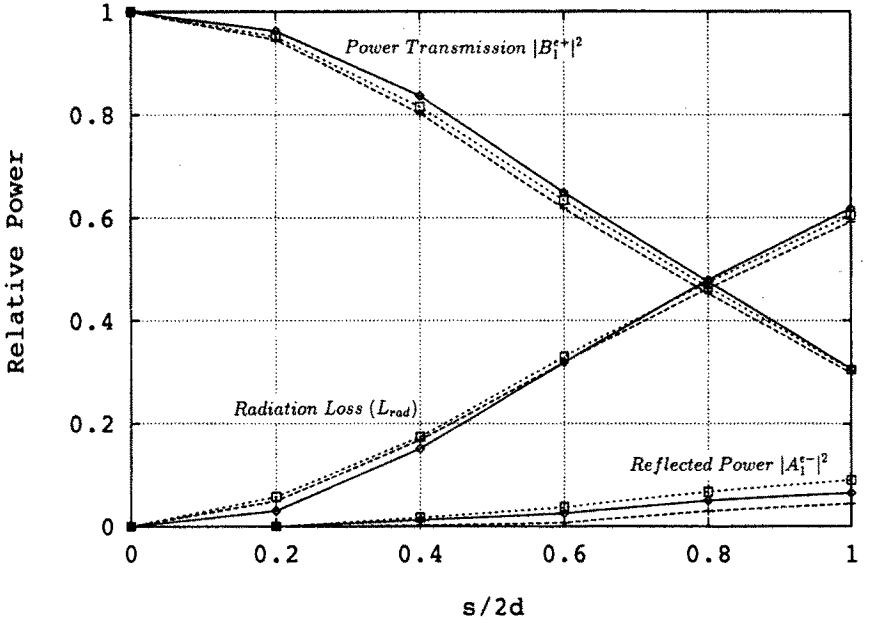

Figure 8. The reflected power $(|A_1^{e-}|^2)$, the power transmission $(|B_1^{e+}|^2)$, and the radiation loss (eq. . 11) of an axially misaligned step junction (Figure 5) between two similar slab waveguides (single-moded) ($d_a = d_b = d, k_0 d = 1., n_1 = n_2 = 1.6, n_3 = n_4 = 1$) by three different methods: P.O. (□), plane wave spectrum (◇), and boundary residual method (+).

Power transmission/reflection and the radiation loss of a junction between two axially *misaligned* dielectric slab (single-mode) waveguides of Fig. 5 are shown in Fig. 8. The dependence on normalized axial displacement $(s/2d)$ as is predicted by the present method is compared with those obtained by a plane wave spectrum technique [41] and the "Boundary Residual Method" [17]. The slab waveguides have small widths $(< \lambda/3)$, but the physical optics (present method) results have very good agreement with those of the other two approaches.

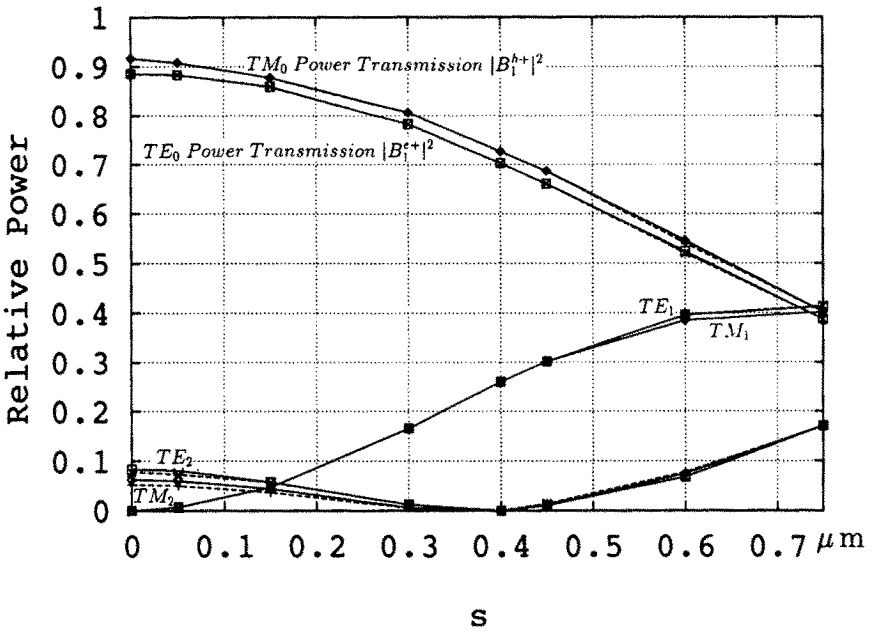

Figure 9. The TE and TM power transmission ratios $(|B_1^{e,h+}|^2)$, $(|B_2^{e,h+}|^2)$, $(|B_2^{e,h+}|^2)$ of a general junction of the type shown in Figure 5 $(n_1 = n_2 = 2.3, n_3 = n_4 = 2.15, d_a = 0.25\mu m, d_b = 1\mu m, \lambda_0 = 1.3\mu m)$ computed by FD/TD (TM:◇, TE:□) and P.O.(TM:+, TE:x).

Fundamental mode power transmission and coupling to *higher order modes* in a general type of asymmetric step junction between two dielectric slab waveguides as a function of the axial displacement s are examined in Fig. 9. Both TE and TM cases have been studied. In both cases, the fundamental mode (TE_0 or TM_0) is coming along the waveguide a. The plots illustrate the variation of the amplitudes of the fundamental mode (TE_0 and TM_0), the first (odd) mode (TE_1 and TM_1), and the second (even) mode (TE_2 and TM_2) in the waveguide b, with the axial displacement. The physical optics results are compared with Finite Difference Time Domain (FD/TD) simulation [42], which is considered to be rigorous, in the Figure 9. Excellent agreement is obtained in all the cases.

5. Abrupt Bends in Dielectric Waveguides (2-D)

A conventional (L–R) symmetrical abrupt bend in a dielectric slab waveguide is a special 2-D version of the general configuration of Figure 1 when $n_1 = n_2, n_3 = n_4, \phi = 90° - \Delta/2$, and there are no step discontinuities on the interface plane which means that Q_1 and Q_3 coincide with Q_2 and Q_4 respectively.

In this section we study a more general structure where the slab waveguides forming the bends, are not similar. The abrupt bend under consideration is now shown in Fig. 10.

The application of the method to conventional abrupt bends in dielectric slab waveguides and a new design including a step change in dielectric index across the interface (SRI) have been described in [25]. In this section we present the essential steps along with some new results on comparison with other techniques.

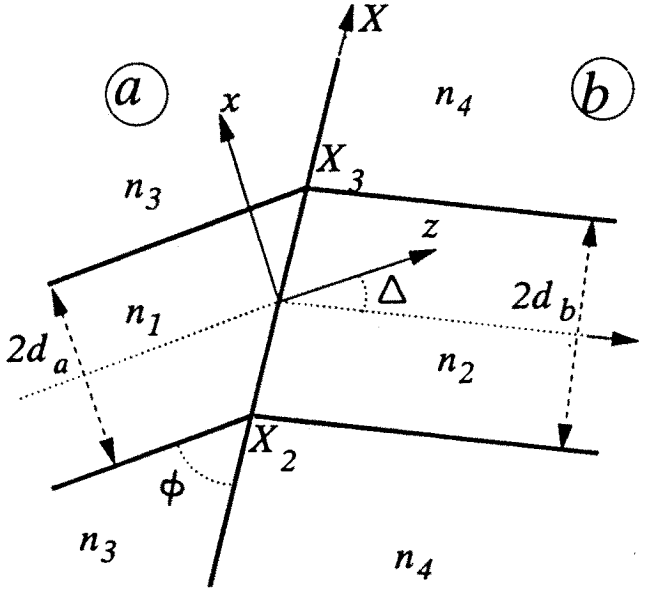

Figure 10. Abrupt bend with two different slab waveguides.

5.1 Transmission and Reflection Coefficients

Consider TE polarization first. A unit power TE ($\vec{E}_a^{inc}$) fundamental mode propagates along the waveguide a towards the junction. We determine the coefficients of coupling to various modes in the waveguide b and the amplitude of the reflected mode(s) in the waveguide a.

The incident field is the same as that in Section 4 and so is given by (13). For convenience we define a coordinate X along the inclined interface in Fig. 10.

Inside the *core* region ($|x| < d_a$ or $X_2 < X < X_3$ along the interface) the incident field can be represented by a sum of two plane waves. Following the procedure described in Section 4 and [25], to find the total P.O. field $\vec{E}_P^{PO}$ at a typical point X on the interface surface P, the reflected waves at X are added to the incident plane waves this yields:

$$\begin{aligned}
\vec{E}_P^{PO}(X) =& \vec{E}_{+\delta_a}^{inc} + \vec{E}_{-\delta_a}^{inc} + \vec{E}_{+\delta_a}^{rfl} + \vec{E}_{+\delta_a}^{rfl} \\
=& \hat{y}\frac{C_1}{2}\left\{\left[1 + R^{TE}(X, \frac{\pi}{2} - \phi + \delta_a)\right] e^{-jk_{+1x}X}\right. \\
&\left. + \left[1 + R^{TE}(X, \frac{\pi}{2} - \phi - \delta_a) e^{-jk_{+1x}X}\right]\right\} \\
k_{\pm 1X} =& \beta_a \cos(\phi) \pm \sin(\phi)
\end{aligned} \tag{31}$$

where the incident and reflected $\pm\delta_a$ plane waves are given by the expressions (16). $R^{TE}(X, \Omega)$ is the *local* TE plane wave reflection coefficient at the interface point X when the incidence direction makes angle Ω with the normal to the interface plane (P) and is again given by (18). However, in contrast to step geometry (Figure 5), here, as is clear from Fig. 10, the interface plane makes an angle ϕ with the z-axis and therefore $\Omega = \pi/2 - (\phi \mp \delta_a)$ for $\pm\delta_a$-rays in (16).

Depending upon the value of X, (n_a, n_b) may assume values (n_1, n_3) and (n_2, n_4) respectively. For the example shown in Figure 10, $n_a(X) = n_1$ and $n_b(X) = n_2$.

In the *cladding* ($|x| > d_a$ or $X < X_2, X > X_3$), the interface field at each point X is again found by summing up the incident and reflected inhomogeneous fields as follows:

$$\begin{aligned}\vec{E}_P^{PO\pm}(X) &= \vec{E}^{inc} + \vec{E}^{rfl} \\ &= \hat{y}C_1 \cos(\tau_a d_a)[1 + R^{TE}(X, \frac{\pi}{2} - \phi \mp \gamma_a)]e^{\alpha_a d_a} e^{-jk_{+1x}X} \\ k_{\pm 3X} &= \beta_a \cos(\phi) \mp j\alpha_a \sin(\phi)\end{aligned} \tag{32}$$

where (+) and (−) signs denote cover ($X > X_2$) and substrate ($X < X_1$) respectively, $\vec{E}^{inc,rfl}$ are given by expressions similar to (21), and $\gamma_a = -\sin^{-1}[j\alpha_a/(n_3 k_0)]$. The reflection coefficient R^{TE} above is given by standard formula (18) but after analytical continuation to complex range of values for $\pm\delta_a$ in the cladding and the substitutions: $n_a(X) = n_3$ and $n_b(X) = n_4$. The arguments related to complex wave vector in (22) and (23) in previous section apply equally well to this case.

P.O. estimate for the magnetic field is obtained by following exactly the same procedure as we used in the Section 4.

The expressions (31) and (32) contain only the contributions of singly reflected waves. It is possible to include the effects of higher order reflected waves [25]. In many practical cases, however, since the reflection coefficients are small, these multiply reflected waves do not have a significant contribution to the total interface fields.

Using the physical optics sources (1) after substituting the fields by the estimates (31) and (32), back in the integral expressions (9) and (10) we can obtain various transmission/reflection coefficients and the radiation loss of the junction. It is interesting to note that, like previous case, all the integrations in (9) and (10) can be carried analytically with the final results casted into closed form formulas.

The closed form formulas for the transmission coefficients for both TE and TM cases along with the contributions of multiply reflected rays are detailed in [25]. The latter contributions, as mentioned earlier, are not significant in many practical applications.

5.2 Accuracy of the Method and Numerical Results

In this section, we present numerical results for some examples and study the accuracy by comparing them with those obtained by other techniques.

In [25] a *symmetrical* conventional abrupt bend in dielectric slab waveguide was chosen for evaluating the accuracy of the method. This

structure is a special case of the geometry depicted in Figure 10, where the waveguides at both sides of the junction are the same ($d_a = d_b, n_1 = n_2, n_3 = n_4, \phi = 90° - \Delta/2$) and located symmetrical with respect to the junction. For this type of bend our physical optics expression for the power transmission ratio $|B_1^+|^2$ given by (9), turns out to be identical with the first iteration solution in a more rigorous iterative numerical procedure described in [23]. The latter was shown [23] to be very accurate. That conclusion also validates our method for treating such problems.

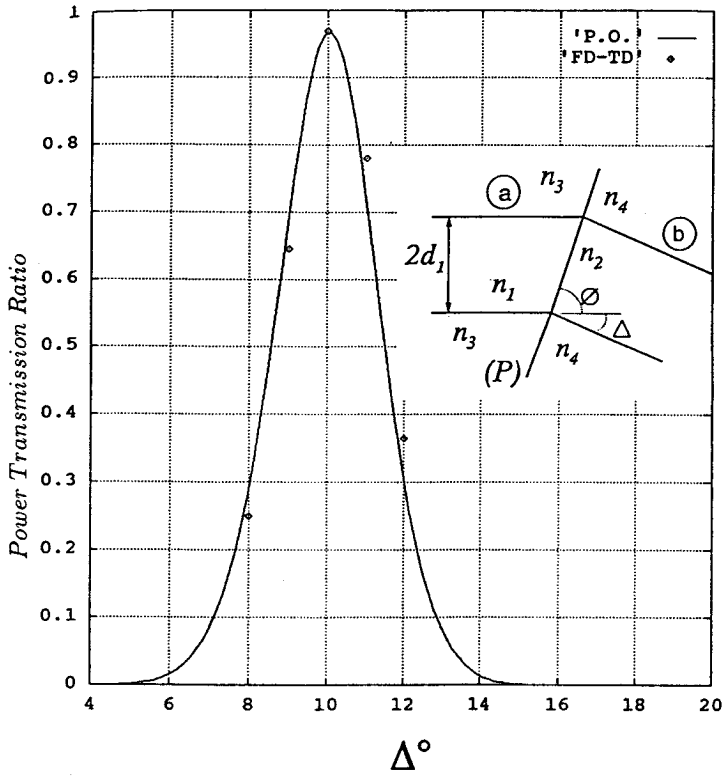

Figure 11. TE power transmission ratio ($|B_1^{e+}|^2$) of a SRI bend ($n_1 = 1.502, n_2 = 1.790, n_3 = 1.5, n_4 = 1.789, d_1 = 3\lambda_0, \phi = 40.0°$) optimally designed to have minimum loss at $\Delta = 10°$ obtained by two methods: P.O. (solid line) and FD/TD ($\diamond$).

To assess the accuracy of the method on a more reliable basis, we compare in Fig. 11 the fundamental *amplitude* transmission ratio $|B_1^+|$ predicted by (9) for a Stepped Refractive Index (SRI) unconventional bend (see Figure 11), with that obtained by the Finite Difference Time Domain (FD/TD) described in [42]. In SRI bends, to redirect the incident wave towards the bent waveguide with minimal loss, the refractive indices are chosen to have step changes across the junction interface plane P. The (SRI) bend under study has been designed according to the criteria (33,34,35), which shall be discussed later, for minimum loss at $\Delta = 10°$. The disagreement between the two methods (normalized to maximum transmission) is less than 5%.

6. Minimum Loss Criteria for Bends Containing SRI Interface

P.O. method provides us with a good insight in not only the cause of the radiation loss of an abrupt bend but also possible approaches to minimize it. From such insight in [25] we proposed a new low loss junction design based on an appropriate change in the refractive index across the junction interface plane P in Figure 10. Such interface, as it was mentioned earlier, is called the *S*tepped *R*efractive *I*ndex (SRI) interface. In this section, we shall discuss the minimum loss criteria of such surface.

6.1 Basic Criteria for Radiation Loss Reduction by a SRI Interface

The radiation loss can be greatly reduced by improving the matching between the field distributions of the incident (plus scattered) wave in the waveguide a and the guiding mode in the waveguide b [25] (see Figure 10). This is particularly obvious from the integral expressions (9) and (10).

To improve field matching and reduce the (bending) radiation losses, following criteria have been proposed [25]:

$$n_1 \cos(\phi) = n_2 \cos(\phi + \Delta) \qquad \text{"Snell's Law"} \tag{33}$$

$$\phi = 90° - \tan^{-1}\left(\frac{n_2}{n_1}\right) \quad \text{"Brewster Angle (TM)"} \tag{34}$$

$$V_a = V_b, \ \frac{n_1}{n_3} \approx \frac{n_2}{n_4} \tag{35}$$

where $V_a = k_0 d_a [n_1^2 - n_3^2]^{-1/2}$ and $V_b = k_0 d_b [n_2^2 - n_4^2]^{-1/2}$ are the normalized frequencies of the waveguides a and b respectively. The equality of the normalized frequencies (35) is a more precise version of the condition (iii) in [25]. A similar condition was stated (without proof) in [43] as a basic guideline for designing low loss *curved* bends and tapers.

The Snell's law implies that paraxial modal rays in the waveguide a refract by the interface P into those of the waveguide b and therefore matches the phase along the interface.

For TM polarization, if the modal rays in the waveguide a have Brewster angle of incidence (see the eq. . 57 in the Appendix), no P.O. reflected field will be generated at the interface and the transfer of power to the waveguide b will be improved.

While the Snell's law results in *phase matching*, the criterion (35) improves the *amplitude matching* between the interface field and the modal field of the waveguide b significantly. To prove this, it may be noted from (14) and (15) that the criteria $(V_a = V_b, n_1/n_3 \approx n_2/n_4)$ lead to:

$$\begin{aligned} \alpha_a d_a &= \alpha_b d_b, \qquad \tau_a d_a = \tau_b d_b (\text{TE}) \\ \alpha_a d_a &\approx \alpha_b d_b, \qquad \tau_a d_a \approx \tau_b d_b (\text{TM}) \end{aligned} \tag{36}$$

for each mode. From the above relationships and the geometric consistency condition: $d_a / \sin(\phi) = d_b / \sin(\phi + \Delta)$,the following equalities can easily be derived:

$$\begin{aligned} \cos(\tau_a X \sin\phi) &= \cos(\frac{\tau_b d_b}{d_a} X \sin\phi) \\ &= \cos[\tau_b X \sin(\phi + \Delta)] \end{aligned} \tag{37}$$

$$\begin{aligned} &\cos(\tau_a d_a) \exp[\alpha_a (d_a \mp X \sin\phi)] \\ &= \cos(\tau_b d_b) \exp\{\alpha_a [d_b \mp X \sin(\phi + \Delta)]\} \end{aligned}$$

for all X . These equalities which are exact for TE modes and nearly exact for TM modes, indicate that the modal distributions of the waveguides a and b are identical or nearly so over the *junction interface plane.* Since the reflection coefficients $R^{TE,TM}$ are often very small and therefore the physical optics estimates for the interface fields are close to the incident modal field, the equalities (37) also imply the *amplitude matching* mentioned earlier. The effectiveness of the design criteria (33,34,35) in minimizing radiation loss is now verified numerically.

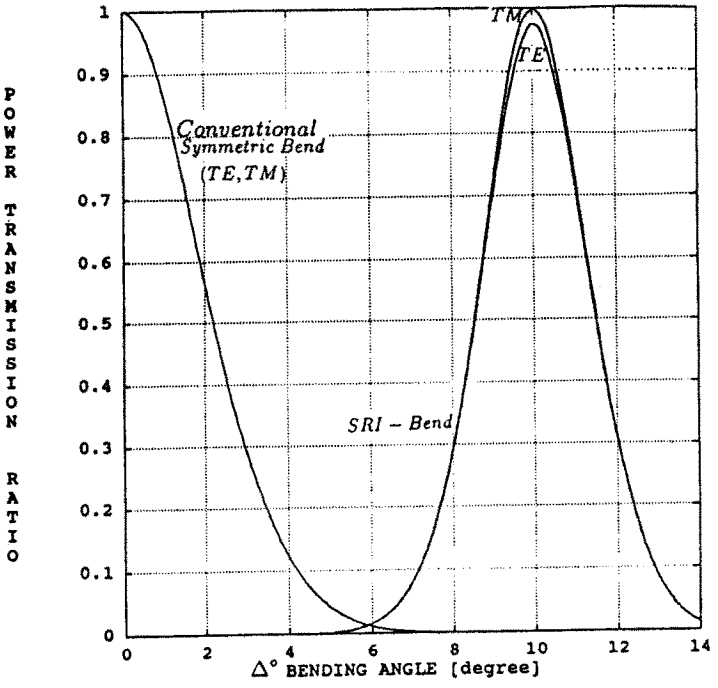

Figure 12. TE power transmission ration ($|B_1^{e+}|^2$) of the SRI bend of Figure 11 optimally designed to have minimum loss at $\Delta = 10°$ compared with that of a conventional symmetric bend ($n_1 = n_2 = 1.502, n_3 = n_4 = 1.5, \phi = 90° - \Delta/2$).

6.2 Numerical Verification

Having established the accuracy of the P.0. method in previous Section, in the following we use this method to examine interesting characteristics of properly designed (SRI) abrupt bends.

The power transmission ratios $|B_1^+|^2$ of the improved (SRI) bend of Figure 11, as a function of the bending angle (Δ) has been plotted in Fig. 12. The same ratios for a conventional symmetrical bend has been included. The plots of the Fig. 12 indicate that the large angle bending loss is minimized by following the design guidelines expressed by the criteria (33,34,35). The significance of the condition (35) is particularly clear from the Figure 13 where the variation of the power transmission ratio of the improved bend has been plotted versus V_b/V_a. In both TE and TM cases, the minimum loss appears around $V_b = V_a$.

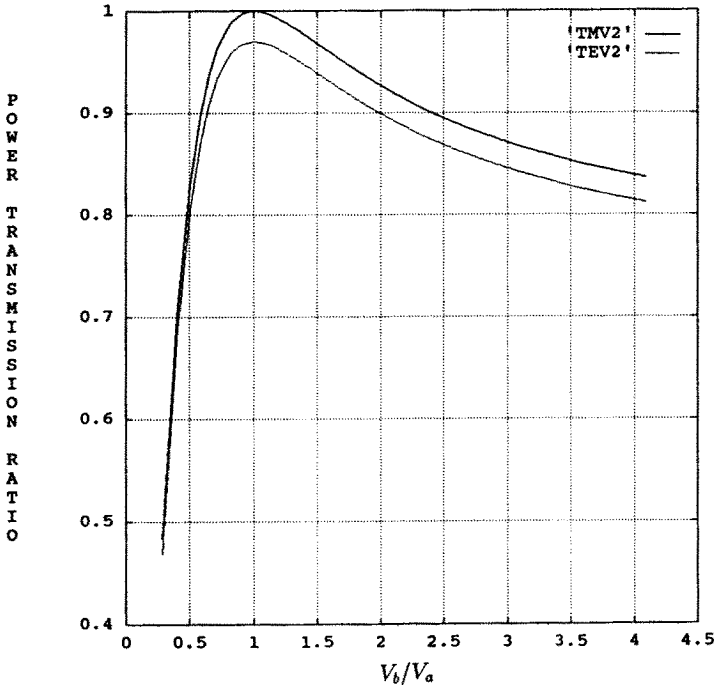

Figure 13. Power transmission rations ($|B_1^{e,h+}|^2$) of a SRI bend of the type shown in Figure 10 ($n_1 = 1.502, n_2 = 1.790, n_3 = 1.5, d_1 = d_a = 3\lambda_0, \phi = 40.0°, \Delta = 10°$) as a function of V_b/V_a (n_4 varies from 1.79 to 1.77) for TM (solid line) and TE (dotted line) cases.

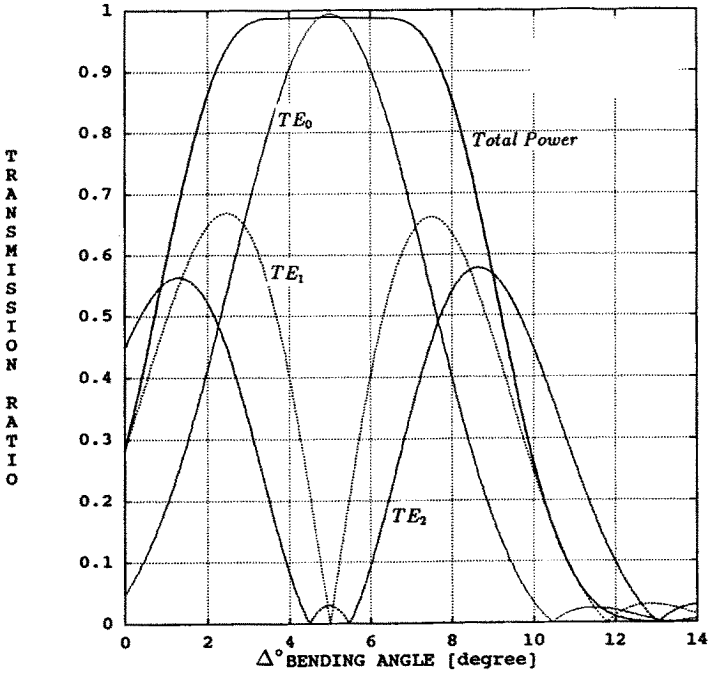

Figure 14. TE mode coupling coefficients $(|B_1^{e+}|, |B_2^{e+}|, |B_3^{e+}|)$ **and the total power transmission** $(|B_1^{e+}|^2 + |B_2^{e+}|^2 + |B_3^{e+}|^2)$ **of the SRI bend of Figure 10** ($n_1 = 1.55, n_2 = 1.833, n_3 = 1.545, n_4 = 1.828, d_a = 3\mu m, \lambda_0 = 0.7\mu m, \phi = 60.0°$).

SRI bend can also be designed to excite higher order modes very efficiently. In multi-mode structures, the coupling between the guiding modes in the waveguides a and b is a function of the bending angle $\triangle$. The amplitudes of the first three TE modes in the waveguide b when the TE fundamental mode incidents along the waveguide a, are shown in Fig. 14. It is interesting to note that the coupling maximum occur when the incident modal rays (waveguide a), upon refraction at the interface, approximately align with those of the guided modes in the waveguide b. The maxima of the couplings to the TE_1 and TE_2 modes are located at $\pm 2.5°$ and $\pm 3.7°$ with respect to $\triangle = 5°$ (maximum transmission bending angle), respectively. These are very

close to the angles of the modal rays of the latter two modes with respect to the axis of the waveguide b, which are 2.7° (TE_1) and 3.9° (TE_2) respectively. This coupling mechanism is very similar to that for excitation of various modes in a large open-ended waveguide when a plane wave illuminates (from outside) its open end [44]. The total power transmitted to the waveguide b is also plotted in the Fig. 14.

A more detailed study of the performance of the SRI bend is given in [25].

7. Y-Junctions in Dielectric Waveguides (2-D)

An extension of the present physical optics method has been used in [26] to analyze and design Y-branches in dielectric slab waveguides. The general Y-branch structure investigated by the authors is shown in Fig. 15. It is actually composed of two bend of the type shown in Fig. 10. A conventional Y-branch is an special case of this structure when $n_1 = n_2$ and $n_3 = n_4$.

In what follows, we describe the physical optics analysis of the general configuration of Fig. 15. The incident field is assumed to be fundamental mode of the waveguide a coming from the left towards the junction. The waveguide a joins two tilted waveguides b and c along two inclined planar interfaces. The amplitudes of the propagating modes in the latter are to be determined.

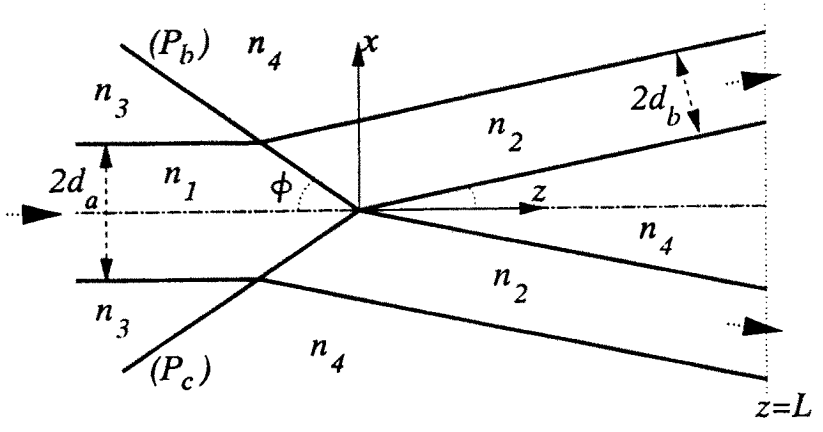

Figure 15. A general symmetric Y-branch with two SRI interfaces.

7.1 Extension of the P.O. Method to Y-branches

To apply physical optics and equivalent principle to Y-branches, the interface surface is taken to be composed of the junction planes (P_b) and (P_c).

The derivation of the P.O. surface fields is similar to that for bends [25] and is detailed in [26]. It is to be mentioned that in the case of Y-junction, the multiple reflections between the interface planes P_b and P_c should be taken into account.

The major difference, however, is that the reciprocity relation (9) cannot be applied directly to a Y-junction. As a matter of fact, the latter expression is only applicable to the cases such as bends or step junctions where the field distribution on the right hand side of the interface (in the absence of the interface and the medium a) has a well-defined modal structure. For other structures like Y-junctions, $\{\vec{E}_m^-, \vec{H}_m^-\}$ must be modified. This point needs some clarification.

The medium on the right hand side of the interface surface $(P_b)+(P_c)$ is not a simple waveguide as was the case in step junctions or abrupt bends. Therefore the expansion (6) may not be a valid representation of the field in this region, especially close to the branching point. However if the branches are sufficiently long and the branching angle (2Δ) is not very small, the interaction between the branches at the output plane is very weak and so the guided wave part of the expansion in (6) may still be used to express the modal field of each branch waveguides in that region. Under these circumstances, over the output plane ($z = L$; L is sufficiently large in Fig. 15), the fields $\vec{E}_{b,c}$ in branches b and c can be represented in terms of a finite sum of the guided modes $\vec{E}^+_{bm,cm}$ of these waveguides in *isolation*:

$$\vec{E}_b(x, L) = \sum_{m=1}^{M_b} B_m^+ \vec{E}^+_{bm}(x, L) \tag{38}$$

$$\vec{E}_c(x, L) = \sum_{m=1}^{M_c} C_m^+ \vec{E}^+_{cm}(x, L) \tag{39}$$

where $M_{b,c}$ are the number of the guided modes in the waveguides b and c respectively and the unguided (radiation) modes are assumed to be negligibly weak at $z = L$. It should be reemphasized that the modal expansions (38, 39) are only valid at distances far from the junction.

To apply reciprocity relation (9) for the Y-junction depicted in Fig. 15, the modal fields $\{\vec{E}_{bm}^{-}, \vec{H}_{bm}^{-}\}$ should be replaced by the interface field for the "reciprocal problem" with wave incidence as illustrated in Fig. 16. In this problem, the incident fields are modal waves of the branch waveguides b and c propagating from the far right (output plane $z = L$) towards the junction, *in the absence* of the SRI interface. Despite this, the field on the junction planes P_b and P_c is evidently not a simple sum of these modal waves. The interactions due to the proximity of the walls of waveguides b and c at the branching region must be taken into account.

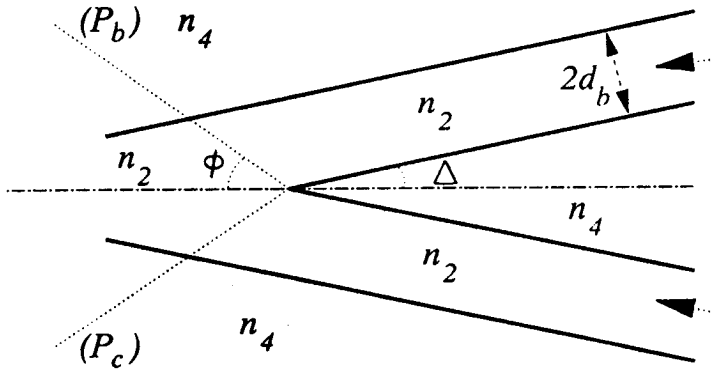

Figure 16. The equivalent problem for determination of the modal amplitudes of the transmitted fields in the branches (reciprocal problem).

The interaction between the adjacent walls of the waveguides b and c can be modeled by evanescent rays [45,46] from one wall, say at b, generating P.O. sources on the other wall, say at c. These P.O. sources in turn radiate (with cylindrical Green's function) onto the (SRI) interface. This extra field due to the proximity effect is then added to the modal fields to give the total P.O. fields (E_{by}, H_{bX}) on the SRI interface. Thus for the especial case of a symmetrical junction under TE (E_y) excitation, the reciprocity relation (9) for the pth mode in guides b and c has the form:

$$B_p^+ = C_p^+ = \frac{1}{2N_{bp}} \int_0^\infty (E_{ay} H_{bX} - E_{by} H_{aX}) dX \tag{40}$$

where (E_{ay}, H_{aX}) are the tangential field distributions over the interface due to the *unit power* incident modal wave from the waveguide a *at the left* and (E_{by}, H_{bX}) are the above mentioned P.O. estimates for the interface fields (i.e., equivalent currents) due to p th modes of the waveguides b and c propagating from the far right in the reciprocal problem discussed above. The derivations are detailed in [26]. The modal amplitude transmission coefficients B_p^+ (from the waveguide a to b) and C_p^+ (from the waveguide a to c) can be used to find the total power transmission ratio T (single mode operation) as follows:

$$T = \sum_{p=1}^{Mb} |B_p^+|^2 + \sum_{p=1}^{Mc} |C_p^+|^2 \tag{41}$$

7.2 Accuracy of the Method

The accuracy of the method is now examined by comparing its numerical results for a conventional Y-junction (without SRI) with those of the normal mode theory (step approximation) [7] and Volume Current Method (VCM) [14]. We assume only the fundamental mode propagates along the waveguide.

The variations with the core refractive index n_1 and the width of the waveguide a of an ordinary symmetrical Y-junction $(n_1 = n_2, n_3 = n_4)$ have been plotted in Figs. 17 and 18. The junction does not have a tapered transition region and $d_a \approx 2d_b = 2d_c (\phi = 90°)$. The refractive index of the cladding is taken to be $n_3 = n_4 = 1$. The plots of Fig. 17 show that in the case of a moderately wide angle branch $(\Delta = 3°)$, the total power transmission improves when the core refractive index increases (stronger confinement of the field). The Y-junction in Fig. 18 is a narrow angle weakly guiding structure. In both cases the numerical results of the present method has very good agreement with those produced by VCM [14].

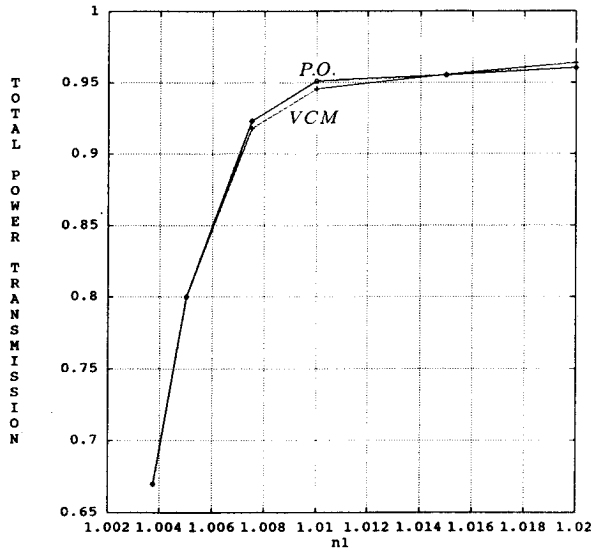

Figure 17. The TE_0 total power transmission of a conventional $(n_1 = n_2, n_3 = n_4 = 1, kd_b = 5, d_a = 2d_b = 2d_c)$ symmetric Y-junction with the branching angle $2\ \Delta = 6°$ as a function of n_1 by two methods: P.O. $(\diamond)$ and VCM $(+)$.

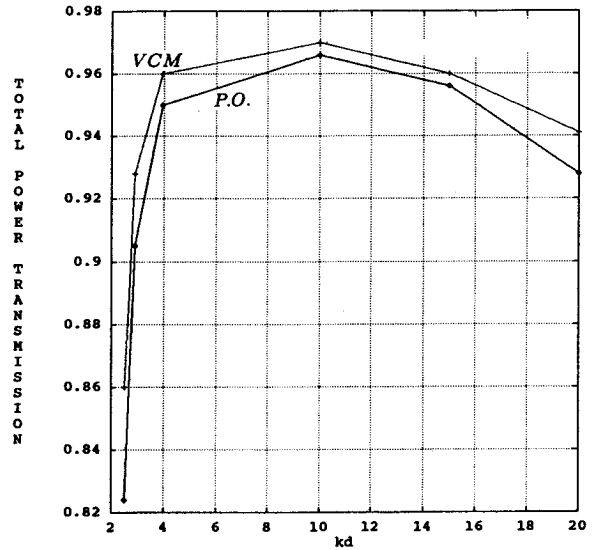

Figure 18. Variation with kd of the TE_0 total power transmission of a conventional $(n_1 = n_2 = 1.003, n_3 = n_4 = 1, d_a = 2d_b = 2d_c = 2d)$ symmetric Y-junction with the branching angle $2\Delta = 2°$ by two methods: P.O. $(\diamond)$ and VCM $(+)$.

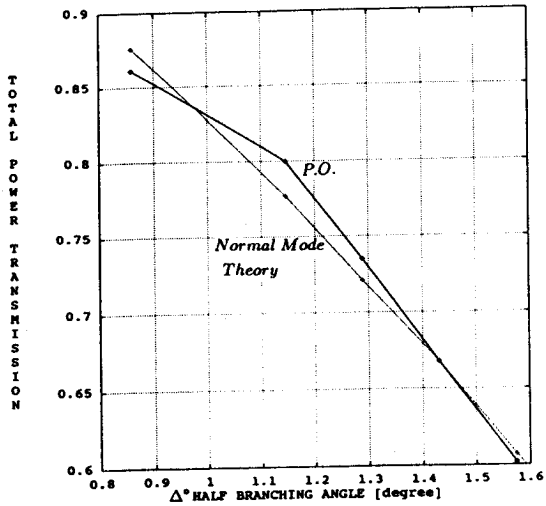

Figure 19. Variation with half branching angle Δ of the TE_0 total power transmission of a conventional symmetric Y-junction $n_1 = n_2 = 1.521, n_3 = n_4 = 1.520, d_a = d_b = d_c = 2.5\mu m, \lambda_0 = 0.6328\mu m)$ computed by two methods: *i*) P.O. ($\diamond$) and *ii*) the normal mode theory with step approximation $(+)$.

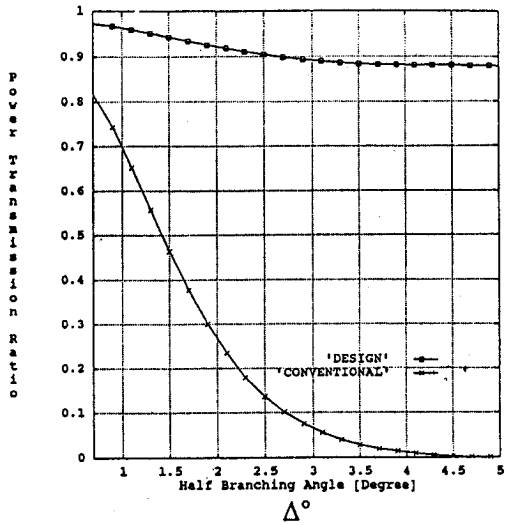

Figure 20. Variation with half branching angle Δ of the TE_0 total power transmission of a conventional symmetric Y-junction $(n_1 = n_2 = 1.521, n_3 = n_4 = 1.520, d_a = d_b = d_c 2.5\mu m, \lambda_0 = 0.6328\mu m)$ compared with that of SRI Y-junction (Figure 15) in which (n_1, n_3, ϕ) follow the criteria (33, 34) and $n_1/n_2 \approx n_3/n_4$.

The Figure 19 illustrates the total power transmission ratio of a symmetrical Y-junction including a relatively long tapered section to achieve a smooth transition between an input waveguide a and two similar waveguides b and c of the same widths ($d_a = d_b = d_c$) The transmission ratio is plotted versus junction half angle Δ. The inclusion of a long tapered section between the input waveguide and the branches was not provisioned in the original version of our method and so its application to this structure required some slight modifications. However, as it is obvious from the Fig. 19, our results agree well with those of the normal mode theory with step approximation [7].

7.3 A Novel Design for Low Loss Applications

In [26], we used the present physical optics analysis method to design and investigate a normal Y-junction structure of the type illustrated in Fig. 15 with $n_1 \neq n_2$ and $n_3 \neq n_4$. Based upon the SRI concept for the abrupt bend, discussed in the Section 6, two interface planes P_b and P_c with step changes in the refractive indices (SRI interfaces) were added at the junction. Then it was shown that if the parameters $\{n_2, n_4, \phi, \Delta\}$ are chosen according to the criteria (33), (34), and $n_1/n_2 \approx n_3/n_4$, the radiation loss will greatly be reduced.

In Figure 20, the TE total power transmission T of a symmetrical conventional Y-junction is compared with that of a (SRI) Y-junction as the branching angle (2Δ) increases from $1°$ to $10°$. The significant transmission improvement is mainly due to better (especially phase 3 matching between the incident (plus scattered at the junction) field and the reciprocal interface field, caused by SRI's.

It is evident from the criteria (33) and (34) that for Y-branches with wider branching angle, larger changes are required in refractive index across the SRI interfaces. For the current state of the art, however, small index changes of the order of 1% are feasible. It was shown [26] that when the relative index changes are of the order of a few thousandths, the Brewster angle criterion (34) is not necessary. By eliminating the latter criterion, SRI wide angle ($2\Delta = 6°\text{to}10°$) Y-junction designs with very small index changes of the order of 0.003 with very low loss became realizable. Some examples of such type were reported in [26].

8. 3-D Structures: Abrupt Bend in 3-D Channel Waveguides, Comparison with Experiment

Many 2-D examples have been discussed thus far. However, the general formulation presented in the Sections 2 and 3 can be applied to 3-D geometries as well. As long as the relevant features of the structure under the study do not have characteristic dimensions much smaller than wavelength, physical optics approximation should produce reliable results.

In this Section after a brief introduction of the main approaches, a P.O. analysis of an abrupt bend in 3-D diffused channel waveguide is outlined. The theoretical results produced by P.O. method applied to a special S-bend, are then compared with available experimental data.

8.1 P.O. Analysis of 3-D Structures

Two basic schema may be followed for treating 3-D structures.

The first and perhaps the simplest scheme, which is particularly appropriate for the 3-D structures supporting paraxial guided waves, is to construct an equivalent 2-D structure with similar propagation characteristics. The methods based on "Effective Dielectric Index" (EDI) concept [47] are possible approaches for this purpose. An example will be discussed later.

A second scheme which is under investigation and is not yet complete, is a two step procedure. First we find the modal field profile of the 3-D structure by some efficient numerical technique and represent it approximately in terms of a finite sum of plane wave rays. In the next step, we use physical optics estimates of the equivalent surface sources for each plane wave constituent in a reciprocity expression similar to (9). The evaluation of the latter expression now involves a 2-D integration over the interface. Although it may be more involved than the 1-D integral for 2-D cases, the procedure is still computationally much faster than the other existing numerical methods.

8.2 Abrupt Bend in 3-D Diffused Channel Waveguide

In [27] we employed an EDI approach to construct a 2-D slab waveguide with the same propagation constant as that of a 3-D diffused channel waveguide. In the following, the essential steps will be discussed.

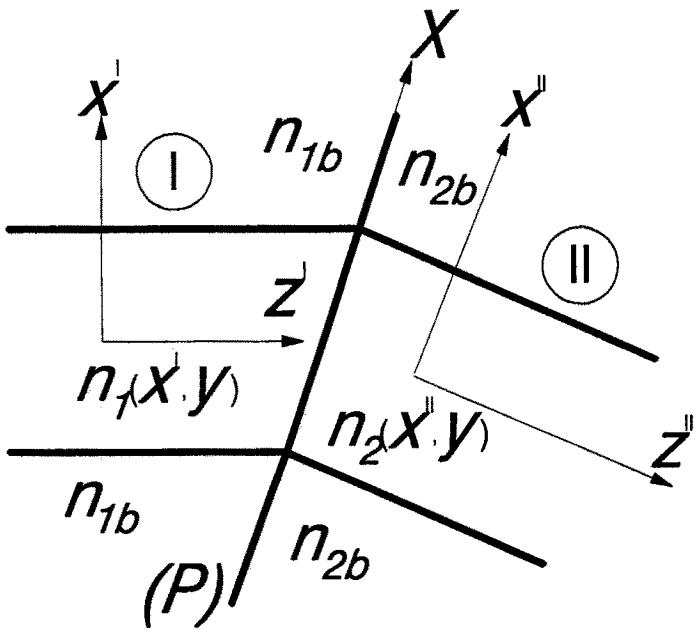

Figure 21. The top view of a general 3-D junction between two different diffused channel waveguides.

The abrupt bend under study is shown in Fig. 21. Two different diffused channel waveguides ($Ti:LiNbO_3$) form a junction with the interface plane (P). The cross section of a 3-D diffused channel waveguide is illustrated in Fig. 22. To model the 3-D bend of Figure 21 by the 2-D junction of Fig. 10, we present a two-step procedure for constructing a 2-D slab waveguide (Figure 23) having the same propagation characteristics as those of the original 3-D guiding structure of Fig. 22.

In the first step we find the propagation constant β and the modal size parameters of the channel waveguides forming the junction (Figures 21 and 22). At this point some preliminary remarks are in order.

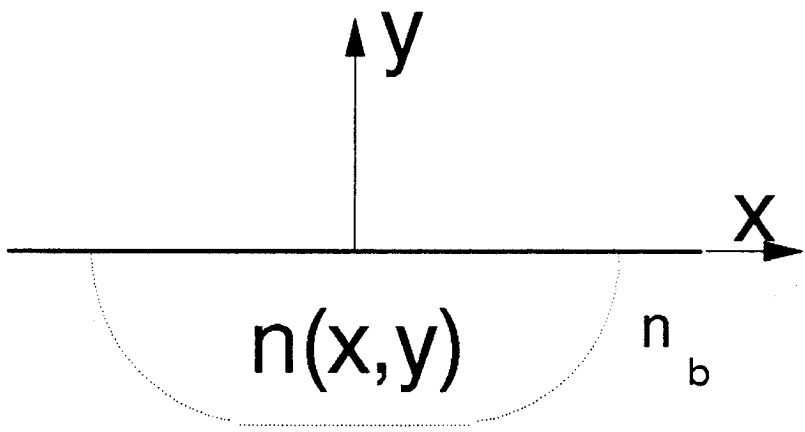

Figure 22. The cross section ($x - y$ plane) of the 3-D diffused channel waveguide.

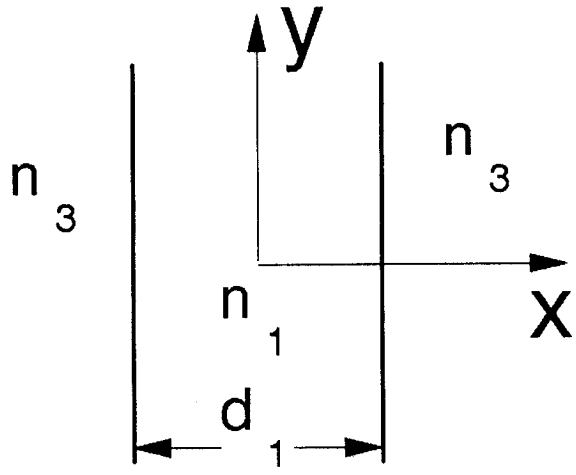

Figure 23. The cross section ($x - y$ plane) of the 2-D equivalent slab.

Diffused channel waveguides are nonhomogeneous guiding media. For the case of diffusion times longer than the time required for complete diffusion of the (Ti) metal strip into the substrate, the refractive index distribution (profile), $n(x,y)$ (see Figure 22), is predominantly Gaussian in depth ($-y$ direction in Figure 22) and complementary error function in width (x direction) [48]:

$$n^2(x,y) = n_b^2 + (n_s^2 - n_b^2) f(y/D) g(2x/W_{st}) \tag{42}$$

where

$$f(y/D) = \exp -(y/d)^2, \quad y < 0$$

$$g(2x/W_{st}) = \frac{1}{2}\left\{ erf\left[\frac{W_{st}}{2D}(1 + \frac{2x}{W_{st}})\right] + erf\left[\frac{W_{st}}{2D}(1 - \frac{2x}{W_{st}})\right]\right\}$$

n_b is the bulk index, n_s, is the surface index, and W_{st} is the width of the metal (Ti) strip before diffusion. The diffusion depth, D, as a function of time t and temperature T is given by $D = 2\sqrt{D_0 t}\exp(-T_0/2T)$ where D_0 and T_0 are some constants.

The corresponding modal field distribution of diffused channel waveguides have been studied both theoretically [49] and experimentally. In the simple case of the isotropic diffusion, it was experimentally shown [50] that the electric field of the fundamental propagating mode in the diffused channel waveguide is approximately a product of a Hermite-Gaussian function along the depth and a regular Gaussian function along the width namely (for TE polarization),

$$E_y^+(x,y,z) = A_0 u(x) v(y) \exp(-j\beta z) \tag{43}$$

$$u(x) = \left[\frac{2}{w\sqrt{\pi}}\right]^{1/2} \exp -\frac{1}{2}\left(\frac{x}{w/2}\right)^2 \tag{44}$$

$$v(y) = \frac{2}{[h\sqrt{\pi}]^{1/2}} \left|\frac{y}{h}\right| \exp -\frac{1}{2}(\frac{y}{h})^2 \tag{45}$$

where w and h (to be determined below) are the modal size parameters of the field along the width (x direction in Figure 22) and depth ($-y$ direction) respectively and A_0 is a normalization constant for unit power.

We compute the above modal parameters using the following variational equation, derived in [51], for propagation constant (or the effective index $N = \beta/k_0$):

$$\Delta N = \left\{ \frac{-3}{2(D/W_{st})^2(h/D)^2} - \frac{4}{2(w/W_{st})^2} + (2n_b\chi_c k_0^2 \zeta_{st} W_{st}) \left(\frac{W_{st}}{D}\right) \times \left[\frac{2}{\pi}\right]^{1/2} \left[1 + \frac{1}{2}\left(\frac{h}{D}\right)^2\right]^{-3/2} \times erf\left(1/\left[(w/W_{st})^2 + 8(D/W_{st})^2\right]^{1/2}\right) \Big/ \left[2(k_0 W_{st})^2 n_b\right] \right\} \tag{46}$$

where $\Delta N = N - n_b$, D is the diffusion depth, n_b is the bulk refractive index, and ζ_{st} is the thickness of the (Ti) metal strip before diffusion. The parameter χ_c is the change in the refractive index per unit change in metal concentration which has been estimated according to the recommendations of [51]. Using the variational properties of (46), we can now determine the modal size parameters h and w by maximizing ΔN for a given diffusion process.

In the second step, we are to construct an equivalent 2-D slab waveguide (Figure 23) which has (i) the same propagation constant (β) and (ii) the same field profile along x-direction as those in the 3-D diffused channel structure of Figure 22. The parameters (n_1, n_3, d_a) of 2-D slab waveguide are found by minimizing the following mean squared difference,

$$\int_{-\infty}^{+\infty} |u_{slab}(x; n_1, n_3, d_a) - u(x)|^2 dx \tag{47}$$

while keeping β constant.

This modeling scheme is used to convert the original 3-D bend of Fig. 22 into an equivalent 2-D (SRI) abrupt bend of the type shown in Fig. 10. The P.O. analysis detailed in Section 5 can now be applied to this equivalent structure.

From our experience the 2-D model usually produces accurate results when the discontinuity (e.g., junction interface plane P in Figure 21) modifies the incident modal field (or rays) primarily in one plane ($x - z$ in our problem).

Performance Analysis of Low Loss S-Bend in 3-D Diffused Channel Waveguide and Comparison with Experiment

In the following, we apply our modeling scheme to the analysis of an especial low loss S-bend in diffused channel waveguide loaded with micro-prisms designed and fabricated by Korotky et al. [52] and shown in Fig. 24. In this S-bend, to minimize radiation loss, the optical path lengths of the inside and outside edges of the bending waveguide is equalized by introducing a series of micro-prisms.

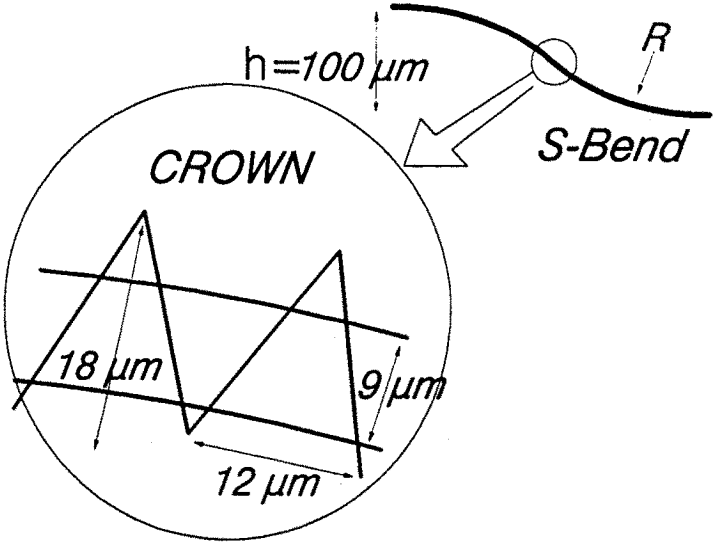

Figure 24. Reduced loss S-bend channel waveguide (3-D) containing microprisms (Korotky et al., [52]).

a) *Micro-Prisms' Losses*

The micro-prisms of the S-bend of Fig. 24 may be considered to be a succession of the junctions of the type shown in Fig. 21. In more detail, the small segments of the curved waveguides inside each prism and between two successive ones can be approximated by short straight sections. The slight abrupt bend formed by two short straight sections meeting at one face of a prism (one outside and the other one inside the prism or CROWN region) may be identified with that in Fig. 21. These 3-D junctions are then modeled by 2-D ones of the type shown in Fig. 10, via the conversion procedure of the Section 8.2.

The total loss incurred for traversing the S-bend is thus determined by summing up the contributions of all these 2-D partial bends.

The 2-D modeling scheme described above is particularly suitable when the radius of curvature is large and the radiation loss of the small curved segments inside and outside the micro-prisms can be neglected. For small radius of curvature, as it will be shown shortly, the accuracy can be improved by adding the bending losses of the intermediate curved sections.

The waveguide and the CROWN region have been designed [52] to result in complete path length equalization (minimum radiation loss) at the bend radius $R \approx 4.0$ mm. The refractive index of the bulk material is around 2.2 and the other parameters of diffusion process for the regions inside and outside the micro-prisms are given in [52]. The index change of the crown region is approximately $\Delta n \approx 0.01$ and the other parameters are shown in Fig. 24.

The exact number of micro-prisms in the fabricated S-bend is not given in [52]. As an estimate for our computation here, the number of micro-prisms is determined by dividing the total length of the S-bend, L_S by the length of the base of each triangle (micro-prism) which is 12 μm for the structure illustrated in Fig. 24. The total length L_S as a function of radius of curvature R is given by $L_S = 2R\cos^{-1}[1 - h/(2R)]$ where $h(= 100\mu m)$ in Figure 24) is the displacement between the input and the output channel waveguides.

The angle of deflection caused by each micro-prism can be obtained approximately by dividing the total arc angle of the S-bend, namely L_S/R, by the number of micro-prisms. One half of this angle gives the bending angle Δ of the 2-D junction of Fig. 10; the latter is the 2-D model for each face of a micro-prism. The inclination angle ϕ in the latter model, for the geometry shown in Fig. 24, is about $71.5°$.

For the specific experimental structure of Fig. 24, at $\lambda = 1.56\mu m$, our theoretical results and the experimental data [52] are plotted in Fig. 25, against the radius of curvature R. From the formulas of the last paragraph it turns out that the refractive indices of the equivalent slab waveguides closely satisfy the criterion (35). It may be noted that in Fig. 25 the model parameter n_4 has slightly been adjusted from the value given by (35), to make our theoretical prediction for largest radius $R = 40$ mm to match the experimental value.

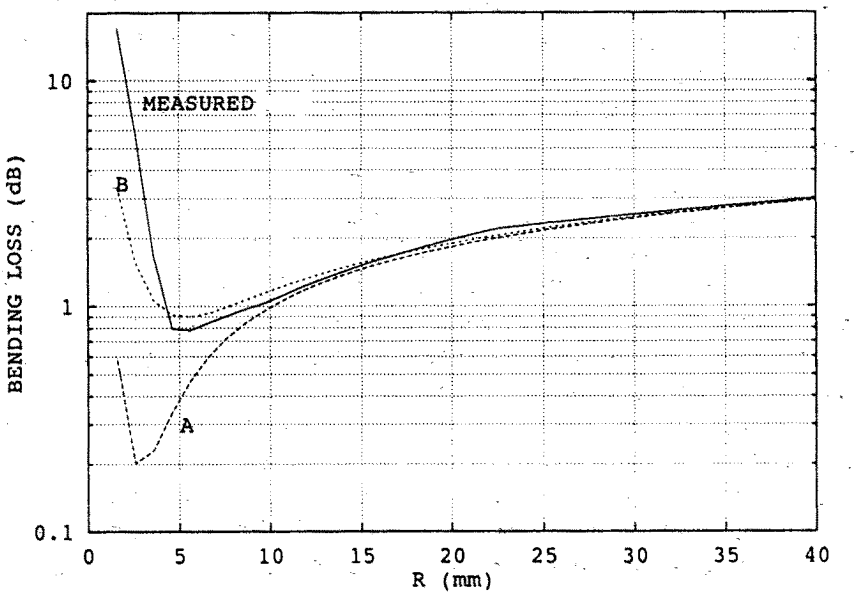

Figure 25. The bending loss of the S-bend illustrated in Figure 24 as a function of the bend radius R: measured (solid line) [52] and theoretical results (plots A and B).

The curve A in Fig. 25 is the result of our simple theory which assumes straight waveguide segments between the interfaces of micro-prisms and thus neglects the small radiation losses of the actual curved segments. The agreement between this theory and the experiment is very good up to the point of experimental minimum loss ($R = 5.5$ mm). Beyond this point to achieve good agreement we need the modeling scheme of subsection b) below.

Before closing this subsection it is of interest to point out that the theoretical (plot A) minimum loss occurs at the radius ($R \approx 3.8$ mm) where the optical path length equalization condition of the micro-prism holds. For *smaller* radii, the reappearing of the phase-mismatch over the micro-prism faces gives a sharp rise in radiation loss which is clearly shown in plot A of Fig. 25.

b) *Additional Loss of Intermediate Curved Sections Without SRI Interface*

The experimental minimum bending loss ("excess loss" in [52]) is observed at a larger radius ($R \approx 5.5$ mm instead of 3.8 mm). This discrepancy is mainly due to radiation losses of the intermediate curved sections neglected in the above theory (plot A in Figure 25). To demonstrated this effect we modeled these sections by another series of partial bends of the type shown in Figure 10 but this time with a symmetric structure and with no prism (i.e., $n_1 = n_2, n_3 = n_4, \phi = 90° - \Delta/2$). The total loss (plot B of Figure 5) is then calculated as the sum of the losses (in dB) of these partial bends and that of the plot A. It is observed that the enhanced model has a good agreement with the experimental data even at small bending radius.

The good agreement with the experimental minimum bending loss gives us a physical insight in the designing of bends, channel or slab, with micro-prisms. The *straight* intermediate sections of waveguides between the micro-prisms, as assumed in subsection a) above, would lead to lower loss compared to the configuration of Figure 24 where these sections are curved. The reason is that a prism designed according to the Snell's law (33) and the equality of the "normalized frequency" V expressed in (35), corrects the phase mismatch across a bend completely whereas in a curved dielectric waveguide the modal phase-front is always distorted. This distortion always causes radiative loss.

9. Conclusions

A physical optics method for analyzing the radiation loss. power transmission, and mode coupling characteristics of the junctions in dielectric waveguides has been presented. The method was based upon using the physical optics estimates of surface fields as equivalent sources in a reciprocity formulation of dielectric waveguide excitation problem. The method has been shown to the insightful, accurate and (computationally) very fast.

Typical applications to 2-D step discontinuities, abrupt bends, and Y-junctions were discussed. The accuracy of the methods in these cases was established by comparing its theoretical predictions with those of more rigorous numerical techniques.

The extension to 3-D structure was also described. Its successful application to a special S-bend structure in 3-D diffused channel waveguide via constructing an equivalent 2-D model, was included. The agreement with experimental measurements has been excellent. The application of the method to several dielectric waveguide junctions, provides us with a clear understanding of their various loss mechanisms.

Appendix: Reflection and Refraction of a Plane Wave from a Planar Interface Between two Dielectric Media

A planar interface between two isotropic, homogeneous dielectric media (with or or without loss) of refractive indices n_1 and n_2, with the unit normal $\hat{n}$ is shown in Fig. 26.

Consider a homogeneous or inhomogeneous plane wave of the form:

$$\vec{E}^{inc} = \vec{E}_0^{inc} \exp(-j\vec{k}^{inc} \cdot \vec{r}), \quad \vec{H}^{inc} = \vec{k}^{inc} \times \frac{\vec{E}^{inc}}{\omega\mu} \tag{48}$$

$$\vec{E}_0^{inc} = (E_{0n}\hat{n} + E_{0u}\hat{u}) + E_{0v}\hat{v}$$

$$\vec{k}^{inc} \cdot \vec{k}^{inc} = n_1^2 k_0^2$$

with the wave vector $\vec{k}^{inc}$ incident upon the interface ($\vec{r} = x\hat{x} + y\hat{y} + z\hat{z}$). The unit vectors $\hat{u}$ (along the interface) and $\hat{v} = \hat{n} \times \hat{u}$ lie on the incidence plane which is formed by the unit normal $\hat{n}$ and the wave vector $\vec{k}^{inc}$.

The plane wave is partially reflected and refracted by the interface. The reflected wave is:

$$\vec{E}^{rfl} = \vec{E}_0^{rfl} \exp(-j\vec{k}^{rfl} \cdot \vec{r}), \quad \vec{H}^{rfl} = \vec{k}^{rfl} \times \frac{\vec{E}^{rfl}}{\omega\mu} \tag{49}$$

$$\vec{E}_0^{rfl} = R^{TM}(E_{On}\hat{n} - E_{0u}\hat{u}) + R^{TE}E_{0v}\hat{v}$$

$$\vec{k}^{rfl} = \vec{k}^{inc} - 2(\vec{k}^{inc} \cdot \hat{n})\hat{n}, \quad (\vec{k}^{rfl} \cdot \vec{k}^{rfl} = n_1^2 k_0^2) \tag{50}$$

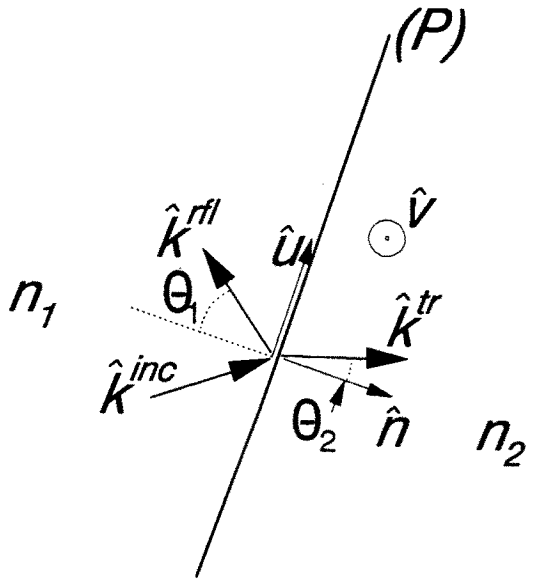

Figure 26. The reflection and the refraction of an electromagnetic plane wave by a planar interface between two homogeneous dielectric media.

The reflection coefficients (R^{TM}, R^{TE}) are given below:

$$R^{TE} = \frac{\hat{n} \cdot (\vec{k}^{inc} - \vec{k}^{tr})}{\hat{n} \cdot (\vec{k}^{inc} + \vec{k}^{tr})} \tag{51}$$

$$R^{TM} = \frac{\hat{n} \cdot (\vec{k}^{inc}/n_1^2 - \vec{k}^{tr}/n_2^2)}{\hat{n} \cdot (\vec{k}^{inc}/n_1^2 + \vec{k}^{tr}/n_2^2)} \tag{52}$$

where $\vec{k}^{tr}$, the wave vector of the transmitted (refracted) wave in medium n_2, is defined by following relations:

$$\vec{k}^{tr} \cdot \vec{k}^{tr} = n_2^2 k_0^2, \quad \vec{k}^{tr} - (\vec{k}^{tr} \cdot \hat{n})\hat{n} = \vec{k}^{inc} - (\vec{k}^{inc} \cdot \hat{n})\hat{n} \tag{53}$$

The important special case of lossless media and an incident wave with a *real* wave vector is discussed next.

Homogeneous plane wave in lossless media

When the incident wave vector $\vec{k}^{inc}$ is real (*homogeneous* plane wave), it is possible to define an *angle of incidence* $\theta_1 = \cos^{-1}(\vec{k}^{inc} \cdot \hat{n}/n_1 k_0)$ between the incident wave vector and the normal to the interface. The relation (50) now expresses the equality of the angle of incidence with the *angle of reflection* (Snell's law of reflection).

If the media are lossless and $n_2 < n_1$ a "critical angle" may be defined as:

$$\theta_c = \sin^{-1}\left(\frac{n_2}{n_1}\right) \tag{54}$$

When $\theta_1 < \theta_c$ the reflection coefficients given in (51) and (52) are real numbers and may be rewritten as:

$$\begin{aligned} R^{TE} &= \frac{n_1 \cos\theta_1 - n_2 \cos\theta_2}{n_1 \cos\theta_1 + n_2 \cos\theta_2} \\ R^{TM} &= \frac{n_2 \cos\theta_1 - n_1 \cos\theta_2}{n_2 \cos\theta_1 + n_1 \cos\theta_2} \end{aligned} \tag{55}$$

where θ_2 is the *angle of refraction* and is given by the Snell's law as below:

$$n_1 \sin\theta_1 = n_2 \sin\theta_2 \tag{56}$$

The expressions (55) are the well-known Fresnel formulas. The expression (18) and (30) have been derived from these formulas.

If θ_1 exceeds θ_c, we have $|R^{TE,TM}| = 1$ and the total reflection of the plane wave occurs.

Another interesting phenomenon is Brewster effect. When the angle of incidence becomes:

$$\theta_1 = \tan^{-1}\left(\frac{n_2}{n_1}\right) = \theta_b, \quad \text{"}Brewster's Angle\text{"} \tag{57}$$

The R^{TM} vanishes (see eq. . 56). This means that TM polarized fields (electric vector in the plane of incidence) propagating along this direction is not reflected at the dielectric interface.

Acknowledgments

This work was supported by the University of Tehran (Iran), Information Technology Research Center of Ontario, and National Science and Engineering Research Council of Canada.

The authors with to thank R. Faraji-Dana and M. Yousefi for checking through final version of the chapter.

References

1. Marcatili, E. A. J., and S. E. Miller, "Improved relations describing directional control in electromagnetic wave guidance," *Bell Syst. Tech. J.*, Vol. 48, 2161–2188, 1969.
2. Marcuse, D., "Radiation losses of tapered dielectric slab waveguides," *B.S.T.J.*, Vol. 49, 273–290, 1970.
3. Taylor, H. F., "Power loss at directional change in dielectric waveguides," *Appl. Opt.*, Vol. 13, 642–647, 1974.
4. Burns, W. K., and A. F. Milton, "Mode conversion in planar-dielectric separating waveguides," *IEEE J. Quantum Electron.*, Vol. QE-ll, 32–39,1975.
5. Sasaki, H., and I. Anderson, "Theoretical and experimental studies on active Yjunctions in optical waveguides," *IEEE J. Quantum Electron.*, Vol. QE-14, 883–892, 1978.
6. Yajima, H., "Coupled mode analysis of dielectric planar branching waveguides," *IEEE J. Quantum Electron.*, Vol. QE-14, 749–755, 1978.
7. Tsutsumi, K., Y. Imada, H. Hirai, and Y. Yuba, "Analysis of single-mode optical Yjunctions by the bounded step and bend approximation," *J. Lightwave Technol.*, Vol. 6, 590–600, 1988.
8. Frenette, N. J. P., and J. C. Cartledge, "The effect of wavefront tilt on mode conversion in asymmetrical Y-branch waveguides," *IEEE J. Quantum Electron.*, Vol. QE-25, 742–748, 1989.
9. Liou, K., U. Koren, E. C. Burrows, M. Young, M. J. R. Martyak, M. Oron, and G. Raybon, "Yjunction power divider in InGaAsP-InP photonic integrated circuits," *IEEE J. Quantum Electron.*, Vol. QE-26, 1376–1383, 1990.
10. Lewin, L., "A method for the calculation of the radiation pattern and mode conversion properties of a solid state heterojunction laser," *IEEE Trans. Microwave Theory Tech.*, Vol. MTT-23, 576–584, 1975.
11. Matsumura, K., and Y. Tomabechi, "Reflection and transmission characteristics of a uncoincidental junction on rectangular dielectric waveguide," *IEEE Trans. Microwave Theory Tech.*, Vol. MTT-37, 414–420, 1989.

12. Nayyer, J., Y. Suematsu, and K. Shimomura, "Analysis of reflection type optical switches with intersecting waveguides," *J. Lightwave Technol.,* Vol. 6, 1146–1152, 1988.
13. Nayyer, J., and S. Safavi-Naeini, "Characteristics of reflection type optical switches with intersecting waveguides: electrode length dependency," *Trans. IEICE,* Vol. E-73, 195–197, 1990.
14. Kuznetsov, M., "Radiation loss in dielectric waveguide Y-branch structures," *J. Lightwave Technol.,* Vol. LT-3, 674–677, 1985.
15. Davies, J. B., "A Least Square Boundary Residual Method for the Numerical Solution of Scattering Problems," *IEEE Trans. on Microwave Theory and Techniques,* Vol. MTT–21, p. 99, Feb. 1973.
16. Mahmoud, S. F., and J. C. Beal, "Scattering of surface waves at a dielectric discontinuity on a planar waveguide," *IEEE Trans: on Microwave Theory and Techniques,* Vol. MTT–23, p. 193, Feb. 1975.
17. Morishita, K., S. Inagaki, and N. Kugamai, "Analysis of discontinuities in dielectric waveguides by means of the least squares boundary residual method," *IEEE Trans. Microwave Theory Tech.,* Vol. MTT-27, 310–315, 1979.
18. Rozzi, T. E., "Rigorous analysis of the step discontinuity in a planar dielectric waveguide," *IEEE Trans. Microwave Theory Tech.,* Vol. MTT-26, 738–746, 1978.
19. Tanaka, K., and M. Kojima, "Volume integral equations for analysis of dielectric branching waveguides," *IEEE Trans. Microwave Theory Tech.,* Vol. MTT-36, 1239–1245, 1988.
20. Baets, R., and Lagasse, "Calculation of radiation loss in integrated-optic tapers and Y-junctions," *Appl. Opt.,* Vol. 21, 1972–1978, 1982.
21. Yevick, D., and B. Hermansson, "Efficient beam propagation technique," *J. Lightwave Technool.,* Vol. 8, 109–112, 1990.
22. Hirayama, K., and M. Koshiba, "Analysis of discontinuities in an open dielectric slab waveguide by combination of finite and boundary elements," *IEEE Trans. on MicrotDave Theory and Techniques,* Vol. MTT-37, 761–768, 1989.
23. Morita, N., "A rigorous analytical solution to abrupt dielectric waveguide discontinuities," *IEEE Trans. on Microwave Theory and Techniques,* Vol. MTT-39, No. 8, 1272–1278, Aug. 1991.

24. Chu, S. T., W. P. Huang and S. K. Chaudhuri, "Simulation and analysis of waveguide based optical integrated circuits," *Computer Physics Communications,* Vol. 68, 451–484, 1991.
25. Safavi-Naeini, S., and Y. L. Chow, "A novel design and analysis of low loss abrupt bends of dielectric slab waveguides," *J. Lightwave Technol.,* Vol. 10, 570–580, 1992.
26. Safavi-Naeini, S., Y. L. Chow, S. K. Chaudhuri, and A. Goss, "Wide angle phase-corrected Y-junction of dielectric waveguides for low loss applications," *J. Lightwave Technol.,* Vol. 11, 567–576, 1993.
27. Safavi-Naeini, S., and Y. L. Chow, "A physical optics analysis for general bends in a 3-D diffused channel waveguide using an equivalent 2-D model," *Optics Communications,* Vol. 96, 59–64, 1993.
28. Snyder, A. W., and J. D. Love, *Optical Waveguide Theory,* Chapman and Hall, chapter 10, 1983.
29. Bowman, J. J., T. B. A. Senior, and P. L. E. Uslenghi, *Electromagnetic and Acoustic Scattering by Simple Shapes,* Hemisphere Publishing Corporation, New York, 29–31, 1987.
30. Yavin, O., and C. W. I. Pistorius, "Bistatic echo-width of a dielectric slab with wedge terminations," *IEEE AP/S Int. Symp. Dig.,* 1570–1573, 1990.
31. Ansorge, H., "Electromagnetic reflection from a curved dielectric interface," *IEEE Trans. Antennas Propagat.,* Vol. AP-34, 842–845, 1986.
32. Uslenghi, P. L. E., *Electromagnetic Scattering,* Academic Press, New York, Chapter 3, 1978.
33. Meixner, J., "The behavior of electromagnetic fields at edges," *IEEE Trans. Antennas Propagat.,* Vol. AP-20, 442–446, 1972.
34. Andersen, J. B., and V. V. Solodukhov, "Field behavior near a dielectric wedge," *IEEE Trans. Antennas Propagat.,* Vol. AP-26, 598–602, 1978.
35. Harrington, R. F., *Time-Harmonic Electromagnetic Fields,* McGraw-Hill, New York, Chapter 3, 1961.
36. Snyder, A. W., and J. D. Love, *Optical Waveguide Theory.,* Chapman and Hall, Chapters 11 and 31, 1983.
37. Collin, R. E., *Field Theory of Guided Waves.,* McGraw-Hill, Chapter 11, 1960.

38. Tamir, T., (Ed.), *Guided-Wave Optoelectronics,* Springer-Verlag, Chapter 2, 1988.
39. Haus, H. A., *Waves and Fields in Optoelectronics,* Prentice-Hall, Chapter 6, 1984.
40. Safavi-Naeini, S., and Y. L. Chow, "A physical optics method of analysis for step discontinuity in dielectric waveguides," to be submitted for publication.
41. Takenaka, T., and O. Fukumitsu, "Accurate analysis of abrupt discontinuity in a dielectric waveguide," *Electron. Lett.,* Vol. 19, 806–808, 1983.
42. Chu, S. T., "Modeling of guided-wave optical structures by the finite-difference time-domain method," Ph.D. Dissertation, Department of Electrical and Computer Engineering, University of Waterloo, Waterloo, Ontario, Canada, p. 88, 1990.
43. Marcatili, E. A. J., "Dielectric tapers with curved axes and no loss," *IEEE J. Quantum Electron.,* Vol. QE-21, 307–314, 1985.
44. Altinas, A., P. H. Pathak, and M. C. Liang, "A selective modal scheme for the analysis of electromagnetic coupling into or from large open-ended waveguides," *IEEE Trans. Antenna propagat.* Vol. AP-36 No. 1 84–96, Jan. 1988.
45. Choudhary, S., and L. B. Felsen, "Asymptotic theory for inhomogeneous waves," *IEEE Trans. Antennas Propagat.,* Vol. AP-61, 827–842, 1973.
46. Einziger, P. D., and L. B. Felsen, "Ray analysis of two–dimensional radomes," *IEEE Trans. Antennas Propagat.,* Vol. AP-31, 870–884, 1983.
47. Robson, P. W., and P. C. Kendall, ed., *Rib Waveguide Theory by the Spectral Index Method,* Wiley, Research Study Press, New York, Toronto, 1990.
48. Hocker, G. B., and W. K. Burns, "Mode dispersion in diffused channel waveguides by the effective index method," *Appl. Opt.,* Vol. 16, 113–118, 1977.
49. Taylor, E. F., "Dispersion characteristics of diffused channel waveguides," *IEEE J. Quantum Electron.,* Vol. QE-12, 748–752, 1976.
50. Keil, R., and F. Auracher, "Coupling of single mode Ti-diffused LiNbO3 waveguides to single-mode fibers," *Opt. Commun.,* Vol. 30, 23–28,1979.

51. Korotky, S. K., W. J. Minford, L. L. Buhl, M. D. Divino, and R. C. Alferness, "Mode size and method for estimating the propagation constant of single–mode Ti:LiNbO3 strip waveguides," [1] *IEEE J. Quantum Electron.*, Vol. QE-18, 1796–1801, 1982.
52. Korotky, S. K., E. A. J. Marcatili, J. J. Veselka, and R. H. Bosworth, "Greatly reduced losses for small–radius bends in Ti:LiNbO3 waveguides," *Appl. Phys. Lett.*, Vol. 48, 92–94, 1986.

[1] Corrected on p. 186 of *Integrated Optical Circuits and Components,* L.D. Hutcheson (ed.), Marcel Dekker Inc., NY, 1987.